LBL-15742

LBL--15742

DE83 009955

DECAYS OF ^{22}AL AND ^{26}P: DISCOVERY OF BETA-DELAYED TWO-PROTON RADIOACTIVITY*

Michael Dean Cable

Ph.D. Thesis

February 1983

Nuclear Sciences Division
Lawrence Berkeley Laboratory
University of California
Berkeley, CA 94720

*This work was supported by the Director, U. S. Office of Energy Research, Division of Nuclear Physics of the Office of High Energy and Nuclear Physics, and by Nuclear Sciences of the Basic Energy Sciences Program of the U. S. Department of Energy under Contract DE-AC03-76SF00098.

Decays of ^{22}Al and ^{26}P: Discovery of Beta-delayed Two-proton Radioactivity

Michael Dean Cable

Department of Chemistry, and Lawrence Berkeley Laboratory
University of California, Berkeley, CA 94720

Abstract:

A helium-jet system and the $^{24}Mg(^{3}He,p4n)^{22}Al$ and $^{28}Si(^{3}He,p4n)^{26}P$ reactions have been used to discover the only known odd-odd, $T_z = -2$ nuclides, $^{22}Al(t_{1/2}\sim70ms)$ and $^{26}P(t_{1/2}\sim20$ ms). Observation of beta-delayed protons from each isotope (laboratory energies 7.839±0.015 MeV and 8.149±0.021 MeV for ^{22}Al and 7.269±0.015 MeV and 6.827±0.050 MeV for ^{26}P) established the existence of these nuclides and provided a measurement of the mass excesses of the lowest $T = 2$ states in their beta decay daughters, ^{22}Mg and ^{26}Si (13.650±0.015 MeV and 5.936±0.015 MeV, respectively). Measurement of these masses confirmed that these $T = 2$ states were unbound to two-proton emission as had been predicted theoretically.

Subsequent proton-proton coincidence experiments, with a specially constructed three-element ($\Delta E1$, $\Delta E2$, E) semiconductor particle telescope capable of simultaneously identifying and measuring proton energies of two protons, enabled observation of the previously unknown decay mode of beta-delayed two-proton emission for each isotope. Two-proton sum energies observed in the decay of ^{22}Al (laboratory energies 5.636 MeV and 4.139 MeV) correspond to transitions from $^{22}Mg^{*}$ ($J^{\pi}=4^{+}$, fed by the superallowed beta decay of ^{22}Al) to the ground state ($J^{\pi}=0^{+}$) and first excited state ($J^{\pi}=2^{+}$) of ^{20}Ne. ^{26}P decay produces an observed two-proton sum group (laboratory energy 4.927 MeV) corresponding to the transition from $^{26}Si^{*}$ ($J^{\pi}=3^{+}$, fed by the superallowed beta decay of ^{26}P) to the ground state ($J^{\pi}=0^{+}$) of ^{24}Mg. Possible mechanisms for two-proton emission are discussed and compared with observed two-proton data. The ^{22}Al decay can not be fully characterized and may consist of components of both ^{2}He and sequential proton emission. The ^{26}P decay observed, however, is spin-parity forbidden to be ^{2}He ($J^{\pi}=0^{+}$) emission and exhibits the expected decay mechanism of sequential emission of two protons.

Decays of ^{22}Al and ^{26}P:
Discovery of Beta-delayed Two-proton Radioactivity

Table of Contents

I. Introduction

In recent years, beta-delayed proton decays of several even-even, $T_z = -2$ isotopes have been studied (for example, (Ay81)). Abundant simultaneous production of $T_z = -3/2$ beta-delayed proton emitters necessitated the use of on-line mass separation for each of these cases. In this work, new techniques were developed for studies of the odd-odd, $T_z = -2$ isotopes, ^{22}Al and ^{26}P.

These odd-odd, $T_z = -2$ isotopes are of special interest since they are thought to be possibly the most proton-rich, particle bound isotope of each element and their existence (or non-existence) is an interesting test of mass prediction techniques. More importantly, however, ^{22}Al and ^{26}P have been found to decay by the exotic modes of decay of both beta-delayed single-proton and beta-delayed two-proton radioactivity. Beta-delayed single-proton decay has been known for about twenty years and is found to occur in virtually all nuclei this far from beta stability; as such, it has become a very useful tool for spectroscopic studies of extremely proton-rich nuclei. It has only been relatively recently, however, that beta-delayed two-proton radioactivity has even been predicted as a potential decay mode (Go80) and this is its first observation.

Studies of beta-delayed single-proton emission of these isotopes were made possible because of the expected high decay energies (7-8 MeV) for protons emitted following the superallowed beta decay of each isotope to the lowest $T = 2$ state in the beta decay daughter. These high proton energies permitted observation of the decays of interest without on-line mass separation, despite the presence of the copiously

produced $T_z = -3/2$ beta-delayed proton emitters. This was useful since current technology would probably not have permitted observation of these isotopes by on-line mass separation.

Observed energies of beta-delayed single-protons from these nuclei provided a measurement of the mass of the lowest $T=2$ analog state in the beta decay daughters. These masses were of interest not only because they provide information on charge dependent effects in nuclei, but additionally, because their measurement confirmed that it was energetically possible for two-proton emission to occur from these levels, as originally predicted by Gol'danskii (Go80). Subsequent proton-proton coincidence experiments permitted observation of this new decay mode.

Observation of this new decay mode opens new possibilities for studies of two-nucleon emission. The analogous process on the neutron-rich side of beta stability, beta-delayed two-neutron decay, has been observed (Az79); however, as shown in this work, charged decay products enable use of techniques by which more detailed information on the mechanisms involved can be obtained.

II. Theory

Before starting searches to investigate a nucleus far from stability, it is necessary to consider several questions, such as: Does the nucleus exist? What are its possible decay modes? What will be some of the characteristics of these decay modes? These questions will be addressed in this section; both a general discussion for light nuclei near the proton drip line, and some specific calculations for the nuclei studied in this work, ^{22}Al and ^{26}P, will be presented.

A. Proton drip line; exotic decay modes

The location of the proton drip line is a question of both theoretical and experimental interest. Theoretical mass models may predict an isotope to be bound (or unbound) to direct proton emission and, in the absence of an actual mass measurement, subsequent experiments to determine particle stability are frequently the only test of the model available. Location of the drip line in the light elements is obviously of interest to the experimenter searching for an isotope through its beta decay modes, since if this isotope "does not exist" no amount of searching is going to be successful.

For the purposes of most decay studies, a nucleus can be said to exist if beta decay dominates; that is, it can even be somewhat unbound to proton emission as long as the proton partial half-life is long compared to beta decay (see Section II-C). For this reason, and for the reason that even the best mass equations are still, after all, only estimates, Figure. II-1 shows nuclei from Z = 10-30 that are

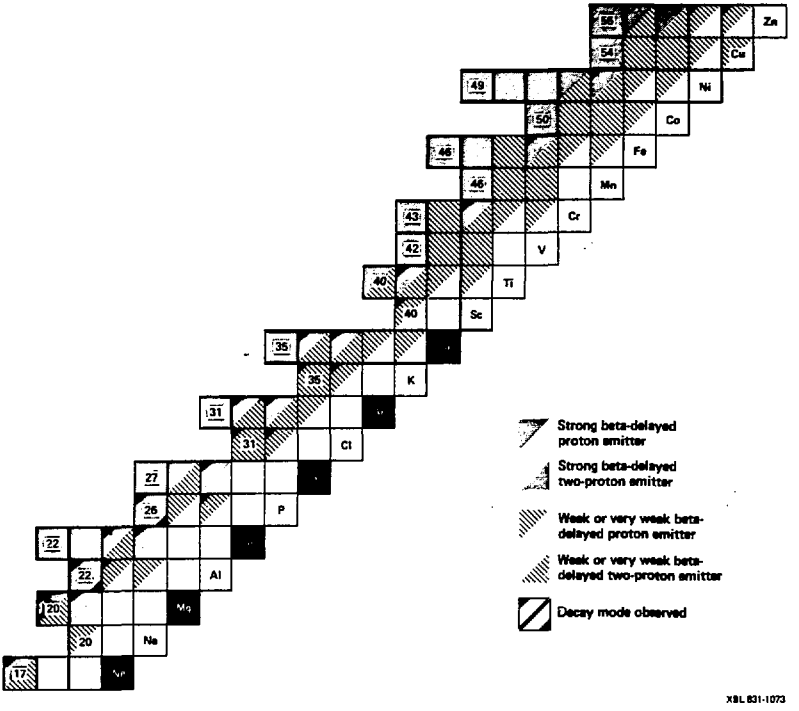

Fig. II-1 Chart of the nuclides showing potential beta-delayed single-proton and beta-delayed two-proton emitters (see text).

unbound to modes of decay other than beta decay by less than the somewhat arbitrary amount of 500 keV. These nuclei are the best candidates for having lifetimes that are observable by techniques used in this work and will therefore be the only ones considered. All masses used to generate this figure are either from the 1982 Wapstra compilation (Wa82) or are generated by the Kelson-Garvey method (Ke66) from masses contained in the compilation.

For light nuclei, as the proton drip line is approached, a number of "exotic" decay modes become energetically possible, in addition to "normal" beta and gamma emission. First, the well-known decay modes of beta-delayed proton and beta-delayed alpha emission become possible. Then, at the very limits of particle stability, it has been proposed that some nuclei will decay by direct single-proton and two-proton radioactivity (Go66). More recently, the new decay mode of beta-delayed two-proton radioactivity has been proposed by Gol'danskii (Go80). Figure II-2 shows a typical decay scheme for a $T_z = -2$ isotope that can decay by both beta-delayed proton and beta-delayed two-proton emission. The decay indicated on the figure involves the superallowed beta decay of the $T_z = -2$ isotope to the $T = 2$ analog state in the emitter. This state is then unbound to subsequent proton or two-proton emission.

Two-proton emission from this state (discussed in more detail in Section II-D) can be compared to the direct two-proton radioactivity mentioned above. In general, the two processes should be quite similar except for a couple of notable differences. First, direct two-proton radioactivity involves emission of two protons from the

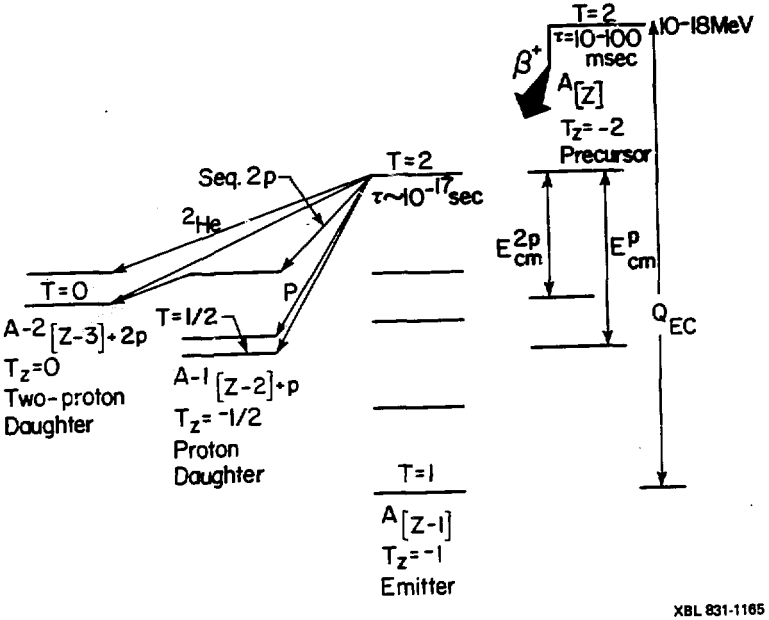

Fig. II-2 A generalized decay scheme for a $T_z = -2$ isotope that can decay by both beta-delayed single-proton and beta-delayed two-proton emission. Single-proton and two-proton decay energies are shown (E^p_{cm} and E^{2p}_{cm}).

ground state of the parent isotope. Usually, two-proton radioactive isotopes are defined to be isotopes in which the direct single-proton decay channel for this state is energetically closed (Go66). This will not be the case for a beta-delayed two-proton emitter; therefore, possible effects such as a sequential emission (see Figure II-2) of the two protons must be considered. Second, two-proton emission from a T = 2 analog state, populated in beta-delayed two-proton emission, will be isospin forbidden. This will have the effect that, despite possible two-proton decay energies of several MeV, this state will be narrow, with a discrete two-proton decay energy.

Generally, beta-delayed two-proton radioactivity is expected to involve the emission of higher energy protons than direct two-proton radioactivity and so makes it a more reasonable goal for an experimental search. Figure II-1 also shows potential, strong beta-delayed single-proton and two-proton emitters. Strong, for the purposes of this figure, is defined such that the analog state, populated by the superallowed branch of the beta decay, is significantly unbound to the decay mode indicated. This does not actually guarantee a large branch since the analog state may decay predominantly by another mode (particularly for two-proton decay; single-proton emission may dominate), but it is a good first criterion. A decay mode is labelled as weak or very weak if it is energetically possible for it to contribute to the decay of the isotope, but it does not fit the definition of strong. Since for some cases the energy available is only a few keV, some of the nuclei

labelled weak or very weak will probably not decay significantly by the decay mode but are indicated for consistency.

It can be seen from Figure II-1 that the odd-odd, $T_z = -2$ series contains the nuclei closest to stability that are potentially beta-delayed two-proton emitters. Of these, ^{22}Al and ^{26}P are the only members below mass 40 that are predicted to be within 500 keV of particle stability. The 1982 Wapstra compilation predicts ^{22}Al to be bound to direct proton emission by 100 keV and ^{26}P to be unbound by 139 keV. Both these nuclei will be shown to exist in this work. Other potentially existing, beta-delayed two-proton emitters which should be a focus of future studies will probably be the higher mass members of the odd-odd, $T_z = -2$ series or the $T_z = -5/2$ series.

B. Beta decay

An expression that is frequently derived for the "comparative" half-life of an allowed beta transition is

$$ft = \frac{K}{G_V^2 \langle 1 \rangle^2 + G_{Ae}^2 \langle \sigma\tau \rangle^2} \qquad \text{(II-1)}$$

where

f = statistical rate function

t = partial half-life

K = 1.230618×10^{-94} erg^2 cm^6 s

G_V = weak interaction vector coupling constant

G_{Ae} = weak interaction axial-vector coupling constant

$\langle 1 \rangle$ = Fermi decay matrix element

$\langle \sigma\tau \rangle$ = Gamow-Teller decay matrix element

Notation for beta decay varies widely; for the most part, that of Raman et al. (Ra78) will be used here.

As it stands, equation II-1 is simplified and needs a number of corrections. Derivation of these corrections is quite complex; a summary of their general nature will be presented with the goal of producing a usable expression for experimental comparison.

Radiative corrections arise from the exchange of virtual photons between the charged particles involved in beta decay. Typically, these are separated into an "inner" radiative correction, Δ_R, and an "outer" radiative correction, δ_R. The inner correction is nuclide independent and is usually incorporated into the vector coupling constant such that:

$$(G_V')^2 = G_V^2 (1 + \Delta_R) \qquad \text{(II-2)}$$

It is actually G_V' that is determined experimentally, so this correction is usually just made by replacing G_V by G_V' and keeping in mind that one is working with an "effective" coupling constant. The outer radiative correction is incorporated into the statistical rate function such that

$$f \rightarrow f (1 + \delta_R)$$
$$\delta_R = \delta_1 + \delta_2 + \delta_3 + \cdots \qquad \text{(II-3)}$$

The δ_i are corrections in i^{th} order of α (the fine structure constant). δ_1 is tabulated in (Wi70) and is less than 2% for most light nuclei. Expressions for δ_2 (Ja70) and δ_3 (Ja72) are

$$\delta_2 \sim 4.0 \times 10^{-4} Z$$
$$\delta_3 \sim 3.6 \times 10^{-6} Z^2 \qquad \text{(II-4)}$$

Radiative corrections also enter into the calculation of f, as do several other corrections such as screening and finite nuclear size. A tabular parameterization of f is given in (Wi74) that not only incorporates all these corrections but is one of the few tabulations that extends to the high beta-decay energies encountered in this work. These corrections also show that the vector rate function differs slightly from the axial-vector rate function, and they will be denoted f_V and f_A, respectively.

The lack of perfect isobaric analog symmetry due to charge-dependent effects is corrected for by modifying the Fermi matrix element such that

$$\langle 1 \rangle^2 \rightarrow \langle 1 \rangle^2 (1 - \delta_c) \qquad \text{(II-5)}$$

δ_c is calculated for many cases in (To77) and is typically less than 1% for light nuclei.

Inclusion of all these corrections in equation II-1 produces the new expression

$$(1 + \delta_R)t = \frac{K/(G_V')^2}{f_V \langle 1 \rangle^2 (1-\delta_c) + f_A R_e^2 \langle \sigma\tau \rangle^2} \qquad \text{(II-6)}$$

From superallowed $0^+ \rightarrow 0^+$ (pure Fermi) transitions a value of G_V' = $(1.4128 \pm 0.0005) \times 10^{-49}$ erg cm^3 can be obtained (Ra78). R_e = G_{Ae}/G_V' is the ratio of the axial-vector and vector coupling constants. Since Gamow-Teller contributions to the decays of interest

for this work are small (see below), renormalization effects in R_e will be ignored and the value from neutron decay of $R_e = 1.237 \pm 0.008$ will be used (Ra78), producing the working equation

$$(1 + \delta_R)t = \frac{6165.4 \pm 4.4}{f_v \langle 1 \rangle^2 (1-\delta_c) + 1.530\, f_A \langle \sigma\tau \rangle^2} \text{ s} \qquad \text{(II-7)}$$

The Fermi matrix element can be shown to be non-zero only for $\Delta T = 0$ transitions and is readily evaluated for superallowed decays by an isospin formalism analogous to that of angular momentum.

$$\langle 1 \rangle^2 = \langle \psi_f | T_\pm | \psi_i \rangle^2 = T(T + 1) - T_{zi} T_{zf} \qquad \text{(II-8)}$$

For the superallowed branches of both ^{22}Al and ^{26}P, $\langle 1 \rangle^2 = 4$.

Evaluation of the Gamow-Teller matrix element is considerably more complex and requires detailed knowledge of the nuclear wavefunctions. At present, this matrix element is best determined through large basis shell model calculations. Such calculations have been done by Wildenthal (Wi82) for the ^{22}Al and ^{26}P decays with the result that $\langle \sigma\tau \rangle^2 = 0.02$ and 0.01, respectively. Since $f_V \sim f_A$ and δ_c is small (see above), the Gamow-Teller contribution to these decays is seen to be negligible compared to Fermi decay and is neglected.

C. Proton emission

Decay rates (or widths) of proton emission for states that are unbound to this decay mode can be described by

$$\Gamma = 2\gamma^2 P_\ell \qquad \text{(II-9)}$$

where Γ is the width and is equal to $\hbar/\tau$ and P_ℓ is the penetrability

of the proton through Coulomb and angular momentum barriers (La58). γ^2 is the reduced width and is dependent on the overlap of the wavefunctions of the initial and final states.

The penetrability is calculable and is

$$P_\ell = \frac{k\,R}{F_\ell^2+G_\ell^2} \qquad \text{(II-10)}$$

where

$$k = \frac{(2\mu E)^{1/2}}{\hbar}$$

$$R = r_o(A_1^{1/3} + A_2^{1/3})$$

F_ℓ and G_ℓ are the regular and irregular solutions to the Schrodinger equation with a Coulomb potential. These values (and subsequently P_ℓ) are calculated by the program COCAG (Se73).

The reduced width is a more difficult quantity to calculate because it depends on wavefunction information; it is frequently parameterized by

$$\gamma^2 = \theta^2\gamma_w^2$$

$$\gamma_w^2 = \frac{3}{2}\frac{\hbar^2}{\mu R^2} \qquad \text{(II-11)}$$

where γ_w^2 is the Wigner sum rule limit and θ^2 is between zero and one (Ma68). This effectively gives an upper limit for γ^2.

Both for proton emission from excited states fed by beta decay and for direct proton emission of a nuclide the quantity of interest is usually the proton partial half-life given by

$$t_{1/2} = \frac{\hbar\,\ell n2}{2\gamma^2 P_\ell} = \frac{\mu R^2\,\ell n2}{3\hbar\,P_\ell\theta^2} \qquad \text{(II-12)}$$

As discussed in the previous section, ^{26}P is predicted to be slightly unbound to direct proton emission. Calculation of the proton partial half-life for ^{26}P evaluates the extent to which this nucleus could be unbound to direct proton emission and still be observable as a beta emitter. Figure II-3 is a plot of the ^{26}P half-life vs. the proton decay energy if a beta-decay half-life of 20 ms is assumed. It can be seen that even for the upper limit case of $\theta^2 = 1$, ^{26}P can be up to 50 keV unbound and still decay primarily by beta emission.

D. Two-proton emission

Beta-delayed two-proton radioactivity is a new decay mode that is energetically possible in some nuclei, as discussed in Section II-A. Possible decay mechanisms for the emission of the two protons can be categorized as simultaneous emission or sequential emission. Gol'danskii (Go66) has considered the simultaneous process and has further divided this category into independent or diproton (^2He) emission (defined below). Gol'danskii has shown that if there is an angular momentum barrier to two-proton emission (as is the case for both ^{22}Al and ^{26}P) then ^2He emission is favored relative to independent simultaneous emission. For this reason, only ^2He emission and sequential emission will be discussed in more detail below. Beta recoil effects will be neglected in this discussion since they are quite small.

^2He decay is the emission of a proton pair coupled to a $^1S_0$ configuration. This virtual state has been studied in reaction work (for example, (Co80) or (St79)) and, for our purposes, can probably be

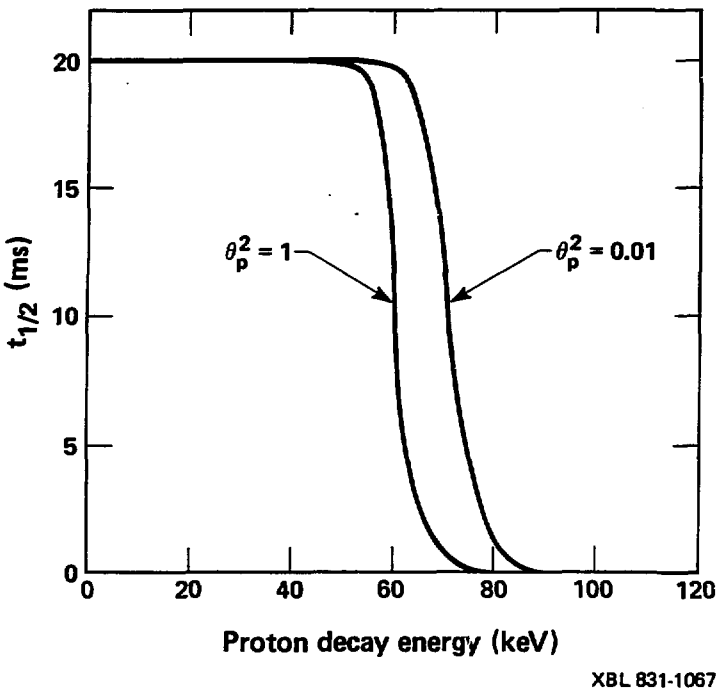

Fig. II-3 Predicted half-life for ^{26}P assuming a 20 ms beta decay partial half-life and ℓ=0 proton emission (see text).

thought of as a proton pair penetrating the Coulomb and angular momentum barriers around the nucleus with a virtual energy ϵ shared between the protons. This center-of-mass energy of the proton pair then "returns" outside the barriers as kinetic energy of tne protons. Since these protons are emitted in opposite directions in the proton pair center-of-mass reference frame, momentum and energy conservation give the following expression for the summed laboratory energy of the two protons:

$$E^{L} = \frac{mE_{cm}+2m_p\epsilon+\epsilon^2}{m+2m_p+\epsilon} \qquad \text{(II-13)}$$

where

E_{cm} = center-of-mass decay energy for the two protons (shown as E_{cm}^{2p} in Figure II-2),

ϵ = relative energy of the two protons (sometimes called the break-up energy),

m_p = mass of proton, and

m = mass of two-proton daughter (for ^{22}Al, mass of ^{20}Ne).

The quantity ϵ is determined by the nucleon-nucleon interaction of tne proton pair (commonly referred to as the final state interaction) and is expected from reaction work (again, for example, (Co80) or (St79)) to appear as a distribution witn a maximum value of ~500 keV and a FWHM of ~600 keV.

Given a value for ϵ, the kinematic expressions for laboratory energies and angles of the protons are a standard problem solved in many texts such as (Sy71) or (Oh65). For tne purposes of this

discussion, it is sufficient to summarize this calculation with the expression

$$\cos\eta = \frac{E_1^L + E_2^L - 2\varepsilon}{2\sqrt{E_1^L E_2^L}} \qquad \text{(II-14)}$$

where

η = the relative laboratory angle between the protons,

and E_1^L, E_2^L = individual proton laboratory energies ($E_1^L + E_2^L = E^L$).

η is maximized for $E_1^L = E_2^L$, and this is also expected to be the most probable value of η. Therefore, the individual proton spectrum from the ^{2}He emission should be a distribution, symmetric about (and probably maximized at) $E_1^L = E_2^L$ with its shape determined by the final state interaction (distribution in ε) and also by the detector efficiency variation as a function of η (see Appendix A).

Sequential emission is a two-step process in which first one proton is emitted to a level in the intermediate nucleus (for ^{22}Al, this nucleus is ^{21}Na), which is unbound to subsequent emission of a second proton. Since this two-step emission is expected to be very rapid compared to detector coincidence techniques, both ^{2}He emission and sequential emission will appear as fast proton-proton coincidences, and mechanistic information on these processes will have to come from kinematic and angular correlation considerations. For transitions where at least one of the protons has $\ell=0$, sequential emission is expected to be isotropic in the center of mass. Since the

recoiling nucleus is much heavier than the protons, sequential emission will also be approximately isotropic in the laboratory for these special cases (such as the major group observed in ^{22}Al decay; see Section IV). Expressions for the laboratory energies of the two individual protons are

$$E_1^L = \left(\frac{m_1}{m_2}\right) E_1 \qquad \text{(II-15)}$$

$$E_2^L = \left(\frac{m}{m_1}\right)(E_{cm} - E_1) + \frac{E_1(m_p)^2}{(m_1)(m_2)} - \frac{2m_p \cos\eta}{m_1}\sqrt{\frac{mE_1(E_{cm}-E_1)}{m_2}}$$

where symbols not in equations II-13 or II-14 are defined as

m_1 = mass of intermediate state
(for ^{22}Al, mass of $^{21}Na^*$)

m_2 = mass of two-proton emitting state
(for ^{22}Al, mass of $^{22}Mg^*$)

E_1 = center of mass decay energy for proton one

It can be seen that the first proton in sequential emission has a "normal" laboratory energy calculated as in single-proton emission but that the second proton laboratory energy is a function of η.

III. Experimental Technique

All of the experiments to be described in this work have one common goal; observation of the beta-delayed proton decay of radioactive isotopes with the production of a permanent record of this information. In general, the process accomplishing this can be described in several steps: 1) production of isotopes, 2) detection of decays, 3) storage of detector information. Each of these steps is a major achievement of modern technology all by itself and is described in more detail below with some (but not all!) of the many variations used from experiment to experiment.

A. Production and transport of isotopes

Production of proton-rich radioactive isotopes below A=40 is usually best accomplished by compound nucleus reactions using proton or ^{3}He beams and Z = N targets. This not only produces the most proton-rich compound nuclei possible in this mass region, but has the advantage that light ion beams are usually available with high intensities. For this work - the production of the odd-odd, $T_z = -2$ isotopes ^{22}Al and ^{26}P - the (^{3}He,p4n) reaction on ^{24}Mg and ^{28}Si was used. Proton beams could also have been employed, but to produce ^{22}Al and ^{26}P with maximal probability requires a high excitation energy in the compound nucleus that can only be obtained with proton beam energies greater than about 70 MeV. Such energies were not available at the facility used (see below), however, useful ^{3}He energies start at about 100 MeV and are readily available.

The facility that provided these ^{3}He beams was the Lawrence Berkeley Laboratory's variable energy, sector-focussed 88-inch Cyclotron. In addition to a variety of other high quality beams, this accelerator is capable of providing intense (up to 10 μA at high energies) ^{3}He beams up to about 135 MeV. Figure III-1 shows the experimental area at the cyclotron. All work described here was done at the location designated CAVE 2, RAMA TARGET. External beams were transported to the Cave 2 area with 80-90% transmission and were focussed to a 3-5 mm diameter for target bombardment.

Nuclides produced in the target must be presented to detectors in a suitable form. For observation of charged particles, this means preparation of a thin source in a vacuum chamber so that particle energy is not degraded by passage through matter. An excellent method for rapid preparation of such a source (half-lives of interest are very short) is the helium jet transport system, shown schematically in Figures III-2 and III-3. Nuclides formed after evaporation of the compound nucleus recoil out the back of the target. The target is located in a box, pressurized to ~1.3 atm of He, which the beam enters and exits through a nitrogen cooled set of double isolation foils. Recoiling isotopes are stopped in the helium and swept through a capillary to a detector chamber. To produce maximum amounts of an isotope, a multiple target, multiple capillary system is sometimes used (see Figures III-2 and III-4). This system (described in more detail in (Mo80) and (Mo81)) has the obvious advantage that several targets produce several times as much activity, with the multiple capillaries providing improved sweep-out of the isotopes.

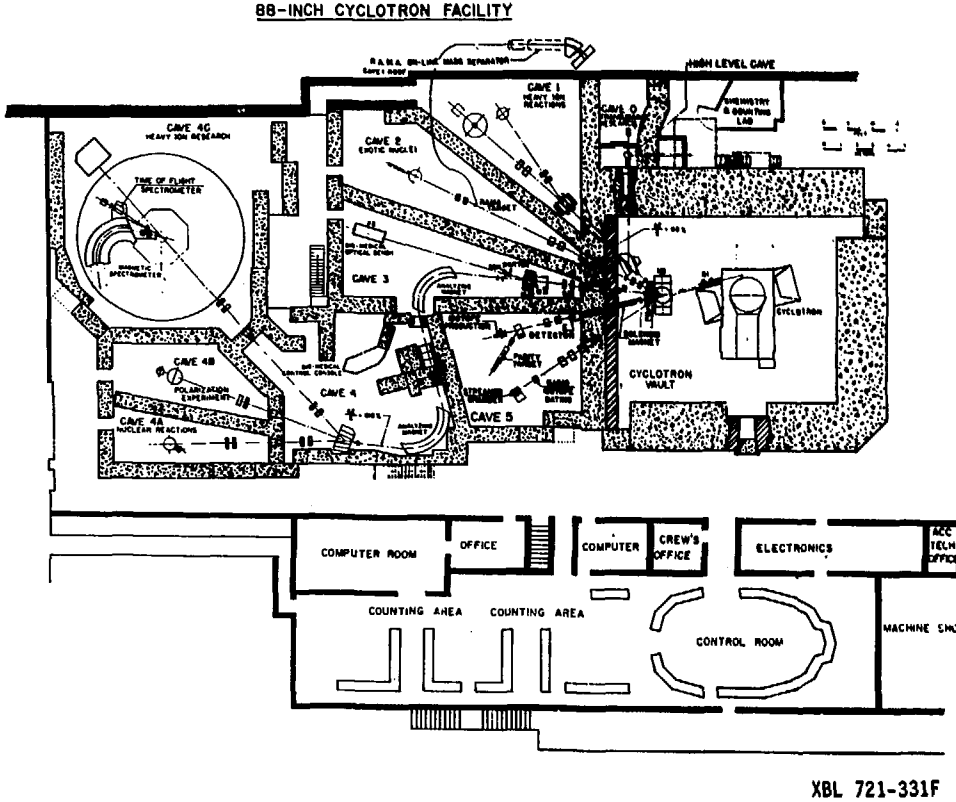

Fig. III-1 Schematic diagram of the 88-Inch Cyclotron facility. All work described used CAVE 2, RAMA TARGET area.

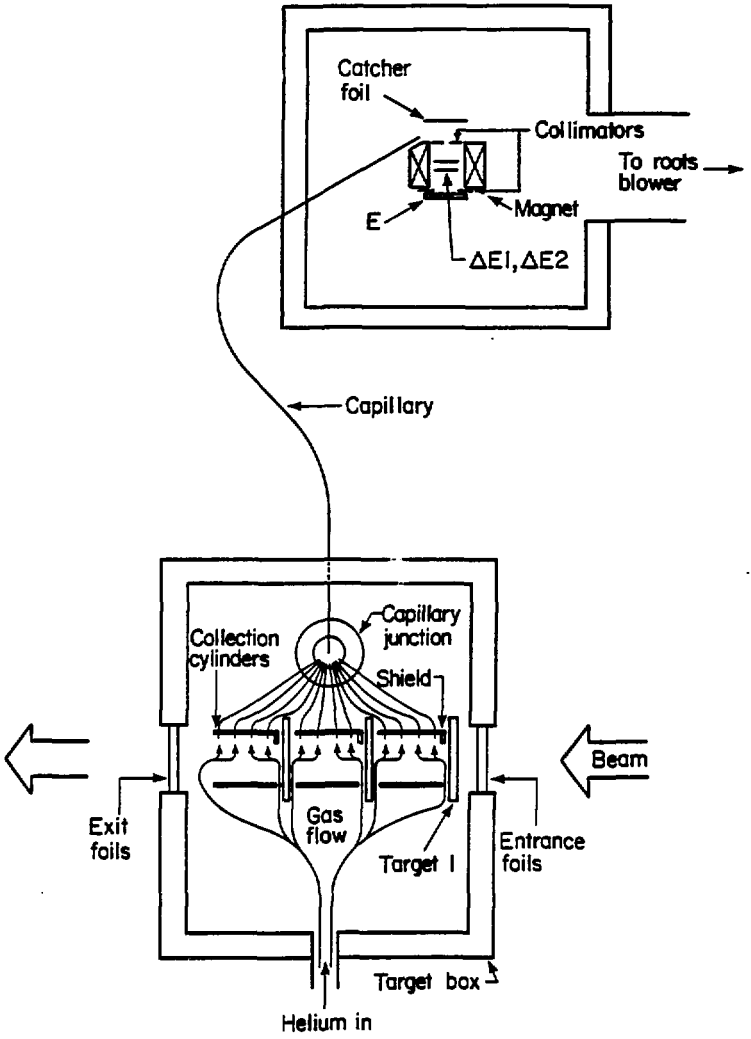

Fig. III-2 Schematic diagram of target and counting chambers. A multiple target, multiple capillary system and three-element single-proton telescope are shown.

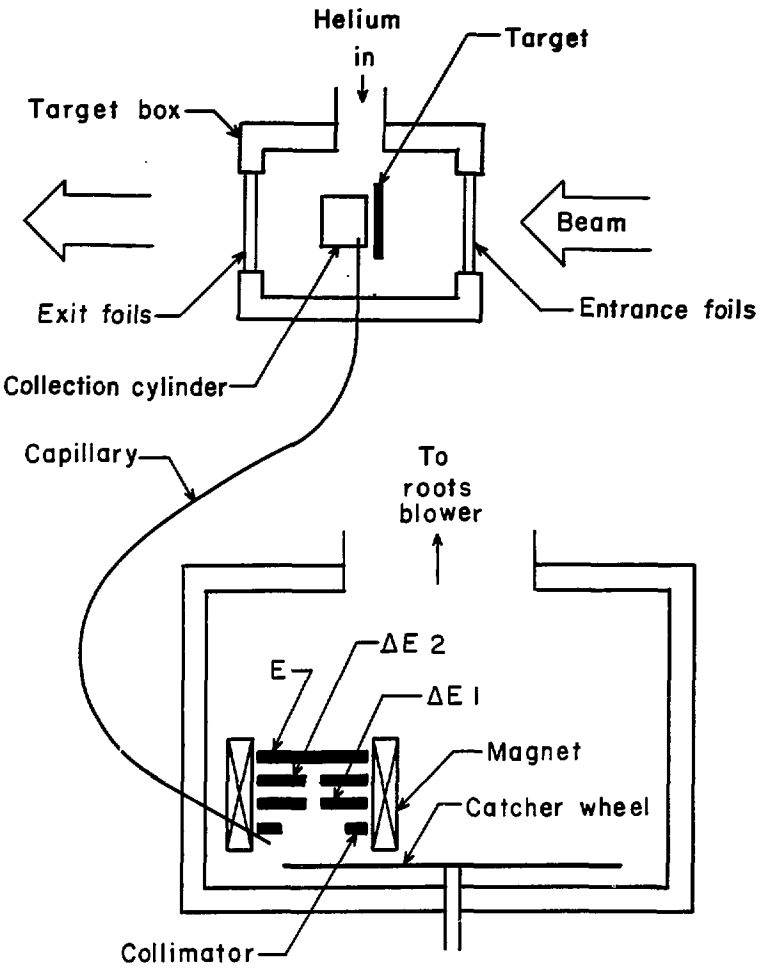

Fig. III-3 Schematic diagram of target and counting chambers. A single target, single capillary system and the two-proton telescope are shown.

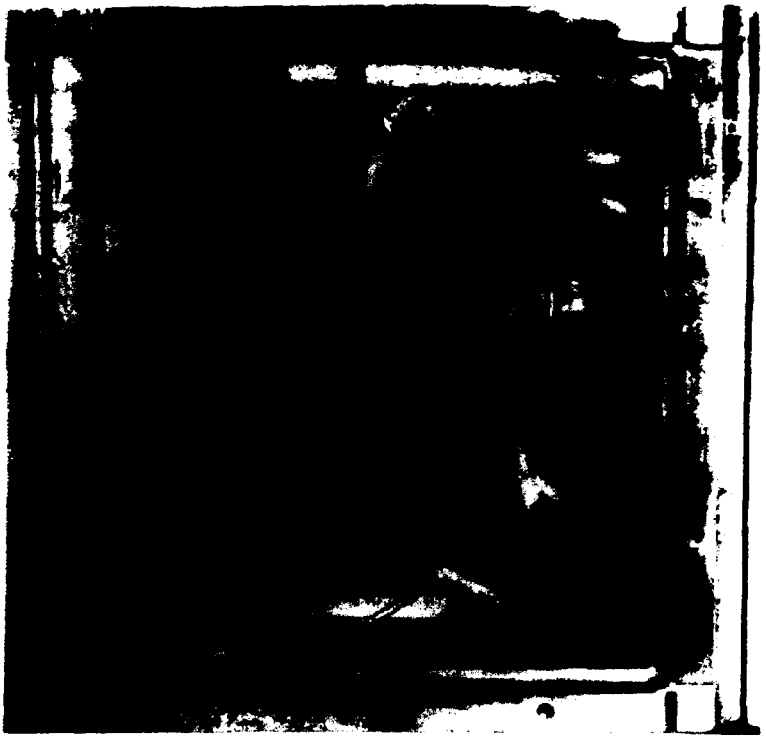

CBB 803-3383

Fig. III-4 Photograph of target chamber showing multiple target, multiple capillary system. Beam enters from right and exits to left.

The major disadvantage of this system is that division of the helium flow through many capillaries slows the gas flow, causing longer transit times (on the order of 100 ms for the 1.1 m long, 1.6 mm i.d. main capillary used) from target to detector chamber. This effect is such that for the half-lives involved in this work (<100ms) higher levels of activity (or at least almost as high) can be obtained with the single target system (transit time probably on the order of 10 ms) shown in Figure III-3. This simple, single target system has a 70 cm long capillary with an i.d. of 1.3 mm. Even if slightly less of the activity of interest is obtained with a single target system (as may be the case for ^{22}Al with the two helium jet configurations shown) there is still an advantage if long-lived activity presents an unwanted interference. If half-life related losses are negligible, so that activity scales proportionally to the number of targets used, a three target system will have three times the long-lived background of a single target system. Long-lived activity did present a problem, as discussed below, so that all but the initial ^{22}Al work was done with the helium jet system shown in Figure III-3.

An important aspect of the helium jet technique is the use of additives to the helium to provide faster and more efficient transport. If large molecular clusters (>10^3 amu) are present in the helium, isotopes that have recoiled from the target attach to these clusters (by a mechanism not fully understood) and the cluster plus isotope combination is what is actually transported by the helium jet. Proper control of the cluster size produces a combination with a molecular weight that transports very well by staying in the center

(high velocity) region of the laminar flow of helium through the capillary.

Clusters can be formed from a variety of materials, but for this work have been predominantly produced from either ethylene glycol (introduced by bubbling helium through the liquid) or NaCl. NaCl is introduced by passing the helium over NaCl heated to 600°C in a tube furnace. Subsequent cooling of the helium and NaCl vapor mixture produces microscopic NaCl crystals which work very well for transport. A distinct advantage of NaCl is the stability and reproducibility of the system and the ease of control of cluster size by simply regulating the NaCl temperature. Most of the work described here employed NaCl for transport. One disadvantage of this additive is that, for long periods of running, NaCl coats everything! This is usually not a serious problem since a water wash followed by an alcohol rinse easily cleans the elements of the system (even the detectors!) and the problem can be minimized by maintaining the furnace temperature no higher than necessary for fast, efficient transport.

Transport by the helium jet ends with collection of the cluster plus isotope combination on a surface (usually referred to as a catcher) to form a source for counting. This catcher can be almost anything and almost any shape. For our purposes, an aluminum catcher with a smooth flat surface was usually used. It is desirable, but not critical, to have this surface normal to the capillary to form the smallest diameter source (source diameters are usually on the order of 1 mm). In Figure III-3, it can be seen that the capillary and catcher

surface are at a 60° angle, although the figure does not show the 15° angle on the edge of the catcher wheel that brings the surface-to-capillary angle to 45°. A system with this angle still produced adequate sources for counting. The catcher wheel in Figure III-3 can be rotated slowly so that long-lived activity is carried away from the detectors while still allowing detection of most of a short-lived activity. This is an important feature since beta-background is a serious problem in these experiments, as discussed further below. Figure III-5 is a photograph of the detector chamber that also shows the location of the target chamber and capillary.

B. Detector systems

With the formation of the source for counting completed, the next step is to identify the beta-delayed protons arising from the decay of the isotopes produced and measure their proton energies. For this purpose, semiconductor particle telescopes were used. Two different telescope designs were used for the single-proton and the two-proton work. The telescope for the single-proton work will be described first.

1) Single-proton system

For the single-proton work, it was anticipated that ^{22}Al and ^{26}P beta-delayed protons would be in the 7-8 MeV energy range and that there would be very few of them relative to the lower energy (<6.5 MeV) known proton groups present from the decays of $T_z = -3/2$

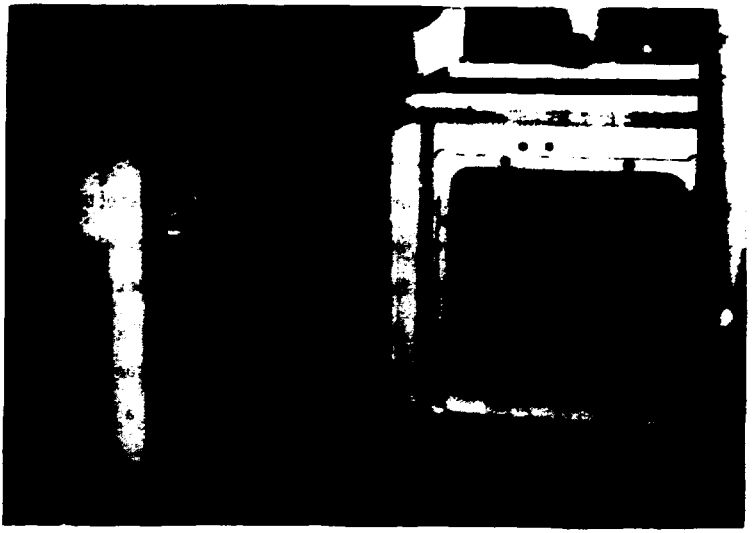

CBB-820-9291

Fig. III-5 Photograph of detector chamber showing two-proton telescope and rotating catcher wheel. Target chamber and capillary are left of detector chamber.

isotopes (Se73) also produced by the reaction used. Anticipated high backgrounds from several sources discussed further below made the use of a three element (ΔE1, ΔE2, E) telescope seem desirable. The 50-100 μm ΔE detectors were fully depleted, P-diffused Si counters fabricated at LBL. All E detectors used were 500-1000 μm Si(Li) detectors, also made at LBL. Such an arrangement had a lower triple coincidence proton threshold of 3.5-4.5 MeV and a high energy limit of 9-13 MeV with exact energies depending, of course, on the actual detector thicknesses chosen for a given experiment. Data collected with this telescope could be analyzed by techniques discussed in Section III-C to produce particle-identified, total energy spectra.

Since the expected counting rate of ^{22}Al and ^{26}P protons was low (on the order of 1 count/hr) it was desirable to use a system subtending a large solid angle ("high geometry"); however, this need had to be balanced with the decreasing quality of data obtained with very high geometry systems. While total energy measurement is not significantly affected by the solid angle of the telescope, several effects can introduce background and/or degrade spectrum quality for a high geometry system. One effect that has already been mentioned is the very high background present from the large number of beta emitters produced. In principle, particle identification (discussed in more detail in Section III-D) can distinguish between protons and beta particles, but in a very high beta background, this is not always the case. Since a beta can "random walk" through a detector, it is possible (but not very probable) for a beta to produce ΔE1, ΔE2, and E energies similar to a proton. With enough betas entering the

telescope, this can be a problem, and since high geometry allows not only more betas to enter but degrades particle identification capabilities, there is a limit to how large a solid angle can be used.

Beta particles can also produce high singles count rates in individual detectors (particularly the thick E detector). If these rates exceed ~10,000 count/s it becomes necessary to use pile-up rejection techniques and if tney exceed ~30,000 cts/s even these techniques can not prevent significant loss of spectrum quality through pile-up between protons and betas. A related "pile-up" effect that is not dependent on counting rate (but is dependent on solid angle) is the simultaneous detection of a beta-delayed proton and its preceding beta. This is not accidental pile-up since these betas and protons are always in coincidence, but the result is the same; with high geometries, proton peaks can have high energy tails that can extend several hundred keV higher than the proton energy.

All of the above beta related effects are, of course, minimized if the betas are physically not allowed to enter the telescope. The rotating wheel previously discussed carries away much of the beta emitting activity before it decays, but can not completely eliminate the betas (we have to let something decay in front of the detectors!). Another method to minimize betas is to install magnets and collimators around the detectors in such a way that betas are deflected into the collimators. Figure III-6 shows a magnet arrangement using Sm-Co permanent magnets. It is possible to achieve a 1-4 kG magnetic field with this type of arrangement. This field does not significantly deflect a proton, but will eliminate some

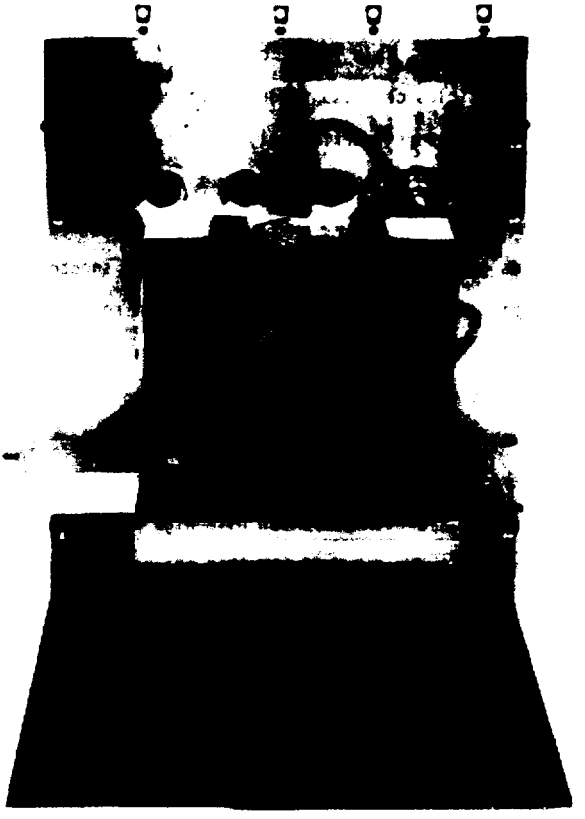

Fig. III-6 Photograph of two-proton telescope. Magnets and entrance collimator (top face) are visible.

CBB 831-507

betas. While the effectiveness of beta removal is not really dependent on solid angle (it is dependent on the distance the beta particles travel through the magnetic field), since detectors have to be a finite size, high geometry means reducing the distance from source to detector and reducing the effectiveness of magnetic removal of betas.

In addition to the above beta-related effects, another background effect was observed that appears to have been caused by high energy neutrons produced by the high energy ^{3}He beam. While the mechanism is not conclusive, our evidence strongly suggests the presence of background caused by high energy neutrons that "knock out" a proton either from matter near the detectors or more probably from an atom of the detectors themselves. These protons, if produced near the front of ΔE1, are indistinguishable from beta-delayed protons and form a continuum of proton energies that can extend to quite high energies. Since most of the neutrons are expected to travel on trajectories at small angles to the beam axis and since it is most likely that a neutron will knock out a proton at a forward angle, this effect can be minimized by orienting the detectors such that the plane defined by the surface of the detectors includes the beam axis (in Cave 2, the detectors are at beam line height and face at the floor). This reduces the effect, but does not eliminate it. The remaining background actually seems to originate from protons knocked out of the thick E detector and passing through the telescope, backward. If the proton stops in the telescope, a "backward" proton is easily distinguished from a "forward" proton by particle identification;

however, it can be shown (see below) that a high energy "backward" proton (~15 MeV) which does not stop, has ΔE1, ΔE2, and E energies very similar to a "forward" proton, making particle identification ineffective.

A spectrum (Figure III-7) obtained during a 110 MeV ^{3}He bombardment of Mg with a 50 μm ΔE1, 50 μm ΔE2, and 1000 μm E and a solid angle of ~0.8% of 4π sr shows an identified proton background extending to ~8.1 MeV. To understand these results, "backward" proton events were studied with the computer code NPEVEN (Ca82), which simulated protons with energies of 5-30 MeV starting at different depths in the E detector and traveling through the telescope backward, thereby accumulating a "test" spectrum. ΔE1, ΔE2, and E energies were calculated by a dE/dx routine and the corresponding particle identification was also computed. If an event had a proton particle identification, it was added to this test spectrum being accumulated.

The test spectrum, totally lacking in any information on the probabilities of producing these neutron induced protons, could not be used to make any judgements about the expected shape of the real background spectrum, but still gave some valuable information. It showed that it was indeed possible for protons traveling backward to produce some type of background (since the test spectrum was not blank) and it showed that for a given telescope, there is a maximum energy to which this background can extend. This maximum energy is a function of all detector thicknesses, but most strongly that of the E detector, and for the ΔE1 = 50 μm, ΔE2 = 50 μm, E = 1000 μm mentioned above, the maximum energy was calculated to be 8.1 MeV.

Another telescope, with ΔE1 = 100 μm, ΔE2 = 50 μm, E = 500 μm had

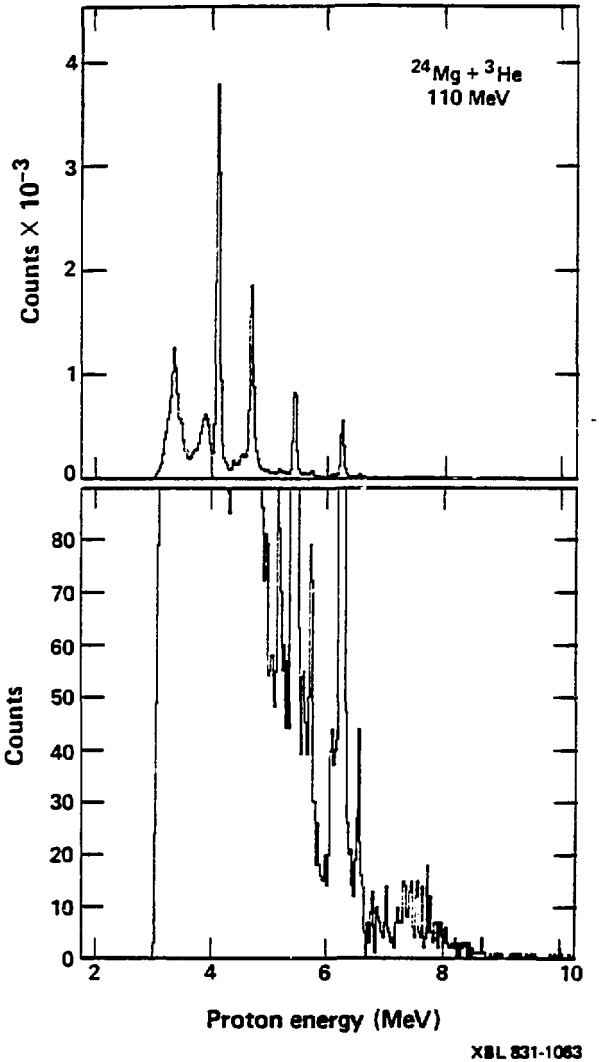

Fig. III-7 Beta-delayed proton spectrum showing protons from decays of ^{21}Mg and ^{25}Si ($\lesssim$ 6.5 MeV) and neutron induced background extending up to $\sim$ 8.1 MeV.

a calculated maximum neutron-induced proton energy of 6.5 MeV and subsequent experiments with this telescope (with a solid angle increased to 1.3% of 4π sr) not only showed a neutron-induced proton background consistent with this calculation but were actually the first experiments in which we observed ^{22}Al (see Section IV-A).

All of the background effects above increase as solid angle is increased (although the neutron-induced protons do not increase as rapidly as one might expect), however, design of a good telescope can be summarized by the statement that "there is no substitute for more data". Experience has shown that if the best efforts are made to minimize all these background effects as described above (and some software techniques described in Section III-D are used) spectrum quality continues to improve with increasing solid angle as long as the ~30,000 cts/s limit in the individual detectors is not exceeded. Original experiments were done with a solid angle of 0.5-0.8% of 4π sr, ^{22}Al was first observed with a telescope subtending 1.3% of 4π sr, and spectrum quality continued to improve in a set-up with 2.3% of 4π sr. Corresponding modifications were made at each step to keep the counting rate down in the E detector (use of a single target system, addition of the wheel, etc.). If further methods are developed to decrease the beta counting rate, it is anticipated that larger solid angles will continue to produce improved spectrum quality.

2) *Two-proton system*

For studies of beta-delayed two-proton emission, it was necessary to develop a detection system capable of simultaneously observing two

protons. Possible mechanisms for two-proton emission were discussed in Section II-D and are of interest here only with respect to possible angular correlations between the protons. If the protons are correlated, for a first detection effort it is obviously best to design a system with peak detection efficiency at the most probable angle between the protons (η). Since sequential emission may be isotropic, possible ^{2}He emission dictated the detector design. Beta-delayed two-proton emission by the ^{2}He mechanism should produce two protons at small angles ($\eta<40^\circ$) and so makes design of a detector that is efficient at these angles desirable.

The detection system developed was a three-element (ΔE1, ΔE2, E) system with many similarities to the single-proton telescope discussed in the previous section, but with the major difference that ΔE1 and ΔE2 are each actually two detectors. Both ΔE1 and ΔE2 were fabricated such that the surface contact on one side of each detector was divided down the center, effectively producing two detectors on the same silicon wafer. For protons stopping in ΔE2, this construction provides two telescopes (a "left" and a "right") capable of detecting two protons simultaneously. Further discussion will refer to these telescopes as left and right but it should be remembered that this is only a form of notation and has no physical meaning. Each side of the ΔE detectors will be referred to as ΔE1-L, ΔE1-R, etc., bringing the total number of detectors in this system to five (ΔE1-L, ΔE1-R, ΔE2-L, ΔE2-R, E). Figure III-3 shows this arrangement schematically and Figures III-5 and III-6 are photographs of the system.

Thicknesses of the detectors used for ΔE1 varied from 14 μm to 31 μm and ΔE2 was typically 155-170 μm thick. Protons with energies from about 1.2-4.5 MeV stopped in ΔE2, providing two two-element telescopes (ΔE1-L and ΔE2-L or ΔE1-R and ΔE2-R) capable of detecting protons in this energy range. Use of a 500 μm E (not split into a left and right detector) produced two three-element telescopes with a lower threshold of about 4.7 MeV and an upper limit of 7-9 MeV (for thinner ΔE1 detectors, the upper end of this range was frequently determined by the low energy threshold in ΔE1; 100 keV was a typical value for this threshold). This arrangement allowed detection of high energy single-proton events with a ΔE1-L, ΔE2-L, E or ΔE1-R, ΔE2-R, E coincidence or lower energy two-proton events giving a ΔE1-L, ΔE2-L, ΔE1-R, ΔE2-R coincidence (See Sections III-C and III-D for a more detailed discussion of the acquisition and analysis of the variety of events that could occur in this system).

Since the left and right telescopes were separated by only a small distance (on the order of 0.1 mm), protons with an angle very close to $\eta=0^\circ$ could be detected. The largest angle that could be detected was about $\eta=70^\circ$ (although efficiency of the detector varies strongly with η as is discussed in Appendix A). Each two-element telescope subtended a solid angle of 4.5% of 4π sr and the two possible three-element telescopes subtended 1.5% of 4π sr each.

Most of the background problems discussed in the previous section also must be considered with this detector system. Magnets and collimators were again used; however, the larger magnet gap necessary in this design lowered the field to ~1.5 kG. All other techniques

discussed in Section III-B(1) were still used to reduce beta particle background. Pile-up rejection techniques were used only with the E detector since counting rates in all other detectors were less than 10,000 cts/s. Despite the numerous background effects previously discussed and the presence of very many low energy protons from T_z= -3/2 isotopes, a proton-proton coincidence is such a powerful requirement in this work that the two-proton spectra obtained with this system have very little (if any) background present.

C. Data acquisition

Both detector systems discussed in the previous section employed similar electronics. Each detector output was amplified first by a charge-sensitive preamplifier with a slow linear output and a fast timing signal which fed separate electronics systems. The slow system further amplified the preamplifier output with a high rate linear amplifier. A logic signal was generated for each detector and sent to a master coincidence system (see below). Each amplified signal passed through a delay gate (gated by the master coincidence system output) to a stretcher (usually set to 2μs) and on to an LBL Multiplexer-ADC unit (see below).

Fast outputs of the preamplifiers were sent to constant fraction discriminators (CFD) to produce a fast timing signal that started and stopped appropriate time-to-amplitude converters (TAC). For both detector systems, the E detector fast signal also fed a pile-up rejector (PUR). The single-proton telescope had TAC's between ΔE1:ΔE2 and between ΔE1:E. The two-proton telescope had TAC's between

ΔE1-L:ΔE1-R, ΔE2-L:ΔE1, ΔE2-R:ΔE1, ΔE2:E. In the latter system, if an L or R was not designated, either side of the detector (L or R) could produce the START or STOP. Additionally, for the two-proton system, a TAC was set up identical to that between ΔE1-L:ΔE1-R except START and STOP were reversed. Since the delays were not changed, this means that for a real proton event STOP comes before START. Such a TAC will only produce an output on a random event and was used to verify the expected low proton-proton random rate of about one random event per 50 hour experiment. All TAC outputs were either strobed by the master coincidence and sent to a stretcher or sent to a gated stretcher (gated by the master coincidence). Stretcher outputs were sent to the Multiplexer-ADC system. Typical timing resolution of these TAC's was better than 10 ns (FWHM).

For the single-proton system a master coincidence was generated each time a triple coincidence between the slow ΔE1, ΔE2 and E logic signals was observed (for some early experiments only a ΔE1, ΔE2 coincidence was required). For the two-proton system, generation of the master coincidence was more complex. The simplest explanation is a FORTRAN logic expression that is TRUE when master coincidence conditions are met

$$((\Delta E1\text{-}L.OR.\Delta E1\text{-}R).AND.(\Delta E2\text{-}L.OR.\Delta E2\text{-}R)) \qquad \text{(III-1)}$$

Basically, this means that if either side of ΔE1 "fires" and either side of ΔE2 fires then a master coincidence is generated. For early experiments this was the master coincidence requirement; however, a

low energy single proton from a $T_z = -3/2$ isotope meets this condition and there were many such protons emitted following the decays of ^{21}Mg and ^{25}Si (and ^{29}S for the ^{26}P work). Since seemingly endless sessions of playing back tapes that are predominantly full of uninteresting events is not a good use of even a grad student's time, the further requirements for a master coincidence were introduced

$$((\Delta E1\text{-}L.AND.\Delta E1\text{-}R).AND.(\Delta E2\text{-}L.OR.\Delta E2\text{-}R)).OR.$$
$$((\Delta E1\text{-}L.OR.\Delta E1\text{-}R).AND.(\Delta E2\text{-}L.OR.\Delta E2\text{-}R).AND.(E)) \qquad \text{(III-2)}$$

Basically, this requirement means that a two-proton event firing both sides of ΔE1 and at least one side of ΔE2 generates a master coincidence or a high energy triple coincidence proton firing one side of both ΔE1 and ΔE2 and firing E generates a master coincidence. Low energy single-protons stopping in ΔE2 would not generate a master coincidence with the above logic. Since these protons are a good monitor of the experiment and can potentially be used for half-life information, branching ratios, cross-section, etc., a sampling was taken of these events. All signals that met the requirements of equation III-1 were sent to a scale-down unit that could sample for example, 2%. Use of this unit enabled the final master coincidence logic to be equation III-2 plus 2% of III-1.

With all parameters of interest and a master coincidence present at the 16-channel LBL Multiplexer, each parameter was individually

sent to a 5 μs analog-to-digital converter (ADC). Digital output was sent to a buffer area of a Mod Comp IV-25 or Classic computer. Magnetic tape recording of event-by-event data and on-line analysis and display (see Section III-D) were handled by the program CHAOS (Ma 79).

D. Data analysis

Analysis of both magnetic tape recorded data and of on-line incoming events was accomplished with CHAOS. Particle identified, total energy spectra could be created and displayed. Total energy spectra varied from the simple ΔE1+ΔE2+E for the single-proton telescope to several different combinations of detectors for the two-proton work. Calibrations for all telescopes were obtained from known groups of $T_z = -3/2$ isotopes (see Appendix C)

Particle identification was accomplished by one or both of two methods. The first was software sorting according to the standard algorithm (Go64)

$$PI \propto (\Delta E+E)^{1.73} - E^{1.73} \qquad \text{(III-3)}$$

For a three-element telescope, either two detectors were summed before using this algorithm or it was used with ΔE2 and E (or, as usually was the case, both techniques were used simultaneously). The second particle identification technique was sorting by generation of a simulated proton (SIMP). The SIMP parameter was obtained through use of the CHAOS FORTRAN expression evaluator and was basically the ratio

of observed proton energy in a given detector to that "expected" for a proton of the observed total energy. "Expected" proton energy was calculated by a dE/dx algorithm generated for any particular telescope by the program DETCAL (Ca82).

Some sorting was aided by use of the program, FILTER (Mc82), which creates new tapes containing only events meeting certain specific requirements (such as a four-fold ΔE coincidence) with a high speed scan of the original data tapes. The resulting filtered data could be sorted with CHAOS much more rapidly than the original data. Sorted spectra were displayed by the program MULTID (Ma79) which is also capable of peak fitting, plotting, and numerous other functions useful for data analysis. The programs SPECTR and PHOTO (Wo82) were also used to plot final sorted data.

IV. Results and Discussion

A. ^{22}Al Decay

^{22}Al was produced via the ^{24}Mg(^{3}He,p4n)^{22}Al reaction with 110 MeV $^{3}He^{+2}$ beams of 3-7 μA intensities. A three target, twelve capillary helium jet system as described in Section II-A was used to transport target recoils to a stationary catcher for the single-proton work and a single target, single capillary system transported recoils to a rotating wheel for the two-proton work.

1) Single-proton data

Proton spectra obtained with a three-element telescope as described in Section III-B (110 μm ΔE1, 60 μm ΔE2, 1000 μm E, 1.3% of 4π sr) are shown in Figure IV-1. At both 60 and 110 MeV ^{3}He energies, the dominant features of each spectrum are due to beta-delayed protons from the decays of ^{21}Mg and ^{25}Si produced via ^{24}Mg(^{3}He,xα2n) reactions; however, at 110 MeV, two new proton groups are observed at laboratory energies of 7.839±0.015 MeV and 8.149±0.021 MeV. As shown in Figure IV-2, these groups can be attributed to the isospin forbidden proton decay of the lowest T=2 state in ^{22}Mg, fed by the superallowed beta-decay of the T=2 ground state of ^{22}Al. Assuming for the moment that the groups do arise from beta-delayed proton decay of ^{22}Al (arguments are presented below), the reasoning leading to the assignment to these particular transitions is as follows:

1) The most probable mass of the state emitting these protons, at least for first consideration, is that obtained by assigning these

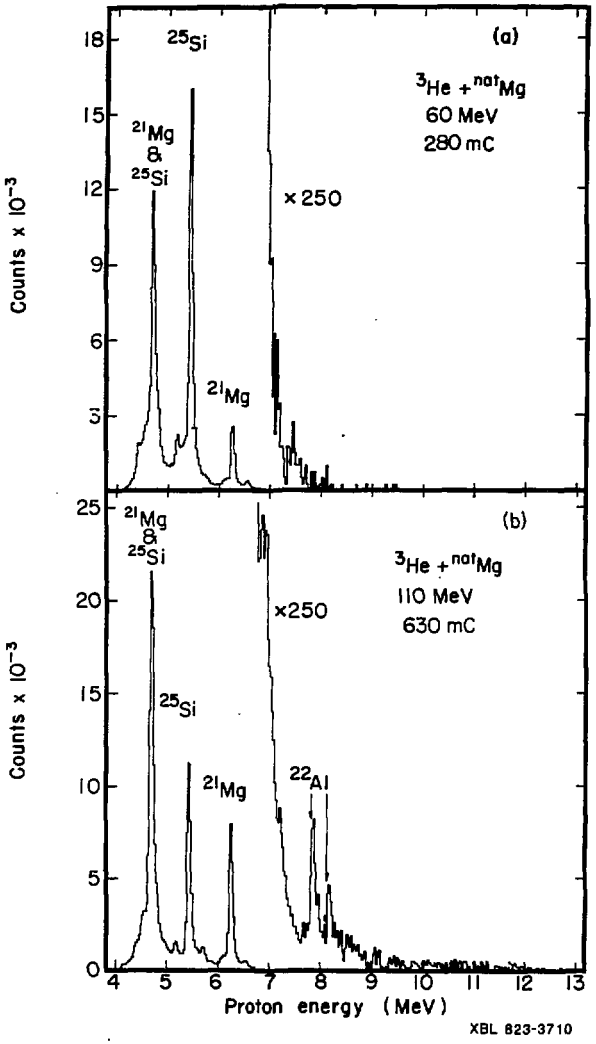

Fig. IV-1 Beta-delayed single-proton spectra. The positions of the arrows labeled ^{22}Al are the predicted energies obtained by using the method of Hardy et al. (Ha69).

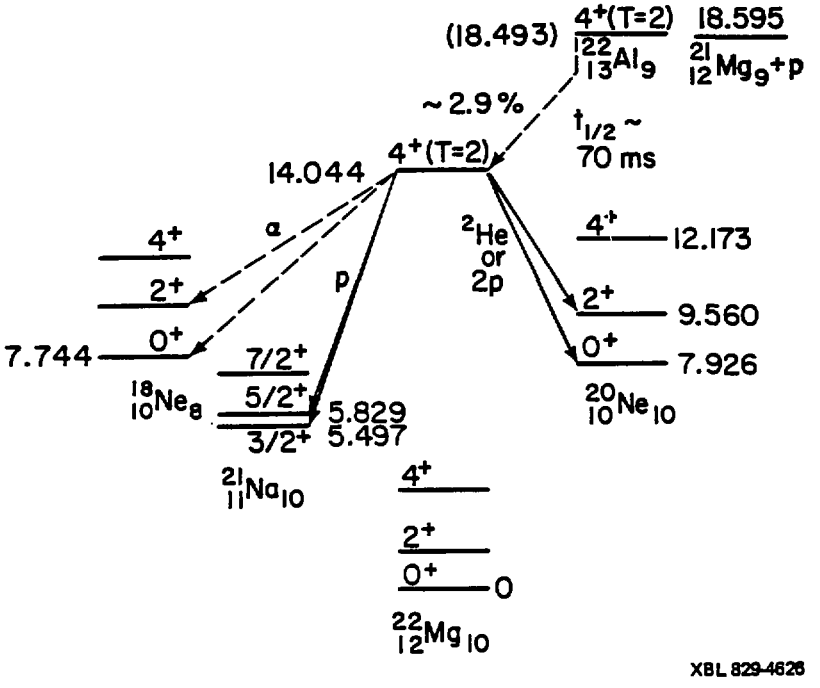

Fig. IV-2 Proposed partial decay scheme for ^{22}Al.

transitions, as indicated in Figure IV-2, to the ground state and first excited state of ^{21}Na. Not only does this provide maximum beta-decay energy for the transition preceding the proton emission, but the relative center-of-mass energy difference between the two observed proton groups is 325±15 keV which agrees very well with the known mass difference of 331.9 keV between the ground state and first excited state of ^{21}Na (En78). Based on the observed energy of the proton group decaying to the first excited state in ^{21}Na and the known ^{21}Na* mass (Wa77), the mass excess of the level emitting the protons is 13.650±0.015 MeV (14.044 MeV excitation in ^{22}Mg).

2) A theoretical mass excess of 13.587 MeV for the lowest T=2 state in ^{22}Mg was obtained by the method of Hardy et al. based on Coulomb displacement energy (CDE) calculations in the $1d_{5/2}$ shell (Ha69) and the ^{22}F ground state mass excess of 2.826±0.030 MeV (St69). This value is very close to that observed, making this state a reasonable source of the observed protons. The arrows in Figure IV-1 are located at the predicted proton energies based on this calculation.

3) Beta decay to other states near this T=2 analog state would have to occur via allowed transitions and would thus be expected to produce considerably less intense proton groups than those following the superallowed decay to the analog state, making groups from decay of the analog state the most probable groups to observe.

The conclusion of these arguments (assuming the protons do arise from the decay of ^{22}Al) is that the decay scheme indicated in Figure IV-2 is almost certainly the correct interpretation. The J^{π}

assignment of 4^+ to the levels in this isospin multiplet, as shown in this figure, is based on the measurement by Davids et al. (Da74) of the $T_z = +2$ member, ^{22}F.

In order to confirm the assignment to ^{22}Al, a spectrum was also obtained at 60 MeV (below the ^{22}Al threshold). This spectrum is shown in Figure IV-1 and does not exhibit the new proton groups after a bombardment of sufficient duration to produce ^{21}Mg and ^{25}Si in quantities comparable to those obtained at 110 MeV. This eliminates ^{21}Mg and ^{25}Si as sources of this activity and also eliminates all nuclei that could have been produced from possible target impurities by high yield ($^3He,2n$) or ($^3He,\alpha 2n$) reactions. All known proton emitters (other than ^{21}Mg or ^{25}Si) with $Z \leq 14$ that could produce protons of ~8 MeV energy would have been identified by known groups not present in the observed spectra. These arguments leave only ^{22}Al and the unknown $T_z=-5/2$ isotope, ^{23}Si, as possible candidates for the source of the new groups.

While some contribution from ^{23}Si cannot be conclusively eliminated, primarily because the predicted mass of the T=5/2 analog state in ^{23}Al (Ha69) is such that proton decay to the second excited state of ^{22}Mg would give an observed proton group at ~7.8 MeV, and also because of the similarity in the ^{22}Al and ^{23}Si reaction thresholds (64 and 61 MeV, respectively), its presence in the spectrum is probably negligible. First ^{23}Si would be expected to have additional, relatively intense beta-delayed proton decays to either one or both of the first excited and ground states of ^{22}Mg (9.8 and 11.0 MeV proton groups, respectively) which are not observed (see

Figure IV-1). Second, as mentioned above, the spacing of the two observed groups is characteristic of the known mass difference in ^{21}Na and would be very difficult to place in a decay scheme for ^{23}Si. Third, the expected shorter half-life of ^{23}Si (~30 ms as opposed to the ~70 ms ^{22}Al half-life, see below) and its expected five times lower cross-section than that of ^{22}Al (based on the evaporation code ALICE (Bl76)) make the observation of ^{22}Al the more likely of the two. Both of the new proton groups are assigned to the decay of ^{22}Al.

A rough half-life (70^{+50}_{-35} ms) for the 7.839 group was determined by observing the relative yields of ^{25}Si, ^{21}Mg and ^{22}Al with different helium jet operating conditions resulting in different transit times from target to catcher. If a helium jet had a discrete transit time for each nucleus transported, this method could, in principle, yield an exact measurement of the ^{22}Al half-life using the ^{25}Si/^{21}Mg ratio as a "clock" to monitor changes. In practice, a helium jet has a distribution of transit t mes, and uncertainties about this distribution together with the low ^{22}Al counting rate yield a measurement with the large error bars quoted (see Appendix B).

A shell model calculation by Wildenthal (Wi82) for the decay of ^{22}Al using allowed branches up to 11 MeV excitation in ^{22}Mg and the superallowed branch yields a predicted half-life of 90 ms. (This should be considered an upper limit on the predicted half-life since there will be some contributions from decays to levels at 11-18 MeV). Assuming a pure Fermi log ft of 3.19 (the Gamow-Teller contribution is negligible, see Section II-B) and using the observed half-life of ~70

ms gives a superallowed branch of $2.9^{+2.1}_{-1.5}$%. Comparison of the ^{22}Al yield to that of ^{25}Si and ^{21}Mg indicates an effective cross-section for the observed proton groups of 1.2 nb (within a factor of three) which corresponds to a lower limit for the total production cross-section of 40 nb. This is a lower limit since not all of the decay proceeds by single-proton emission (see Section IV-A(2)).

As discussed in Section II-A, the ^{22}Al mass is of interest since this nuclide is expected to be at the very limit of particle stability. Using the experimental ^{22}Mg* mass excess and the Haroy et al. (Ha69) value for the ^{22}Al-^{22}Mg* mass difference, a new value of 18.099 MeV for the ^{22}Al ground state mass excess can be predicted, which would make ^{22}Al bound to direct proton emission by only 102 keV. Stokes and Young (St69) have measured the excited states of the ^{22}Al mirror, ^{22}F, and have determined that its first excited state has an excitation energy of 660 keV, indicating that the ground state of ^{22}Al should be its only bound level.

In the same work, Stokes and Young tentatively identified the lowest T=2 state in ^{22}Ne at an excitation energy of 14.07±0.04 MeV. If this assignment is correct, ^{22}F, ^{22}Ne*, and ^{22}Mg* constitute three known members of the mass 22, T=2 isobaric quintet and can be used to obtain the coefficients of the quadratic form of the Isobaric Multiplet Mass Equation (IMME). The IMME (Wi57) can in turn be used as anotner metnod to predict the ^{22}Al ground state mass excess and gives a value of 18.048 MeV indicating that ^{22}Al is bound by 154 keV. Measurements of the mass excesses of the remaining mass 22

analog states (^{22}Na* and ^{22}Al) would be useful to check the IMME for deviations in this A=4n+2 quintet.

2) Two-proton data

Single-proton data discussed in the previous section gave a mass excess for the lowest T=2 state in ^{22}Mg of 13.650±0.015 MeV. Figure IV-2 shows that this value indicates this T=2 level is unbound to two-proton emission by 6.118 MeV.

Coincident two-proton spectra obtained following a 690 mC bombardment by methods discussed in Section III are shown in Figures IV-3 and IV-4. Figure IV-3(a) is a two-dimensional plot of the "left" two-element, low energy telescope (ΔE1-L + ΔE2-L) vs. the "right" one for events identified as proton-proton coincidences in a 20 ns coincidence window. The summed proton energy appears in Figure IV-3(b). Given the 20 ns coincidence window and the observed proton counting rates in each telescope (almost entirely from the T_z=-3/2 beta-delayed proton emitters ^{21}Mg and ^{25}Si), only one random coincidence is to be expected in this spectrum. This expectation was confirmed with a special TAC set-up described in Section III-C.

Laboratory energies of the two-proton total energy peaks shown in Figure IV-3(b) are 4.139±0.020 MeV and 5.636±0.020 MeV. Exact corresponding center-of-mass energies depend on the mechanism of two-proton emission, as will be discussed further below (also, see Section II-D); however, these peaks can be shown to correspond to transitions from the ^{22}Mg T=2 analog state (fed by the superallowed beta decay of ^{22}Al) to the ground state and first excited state of ^{20}Ne (see Figure IV-2).

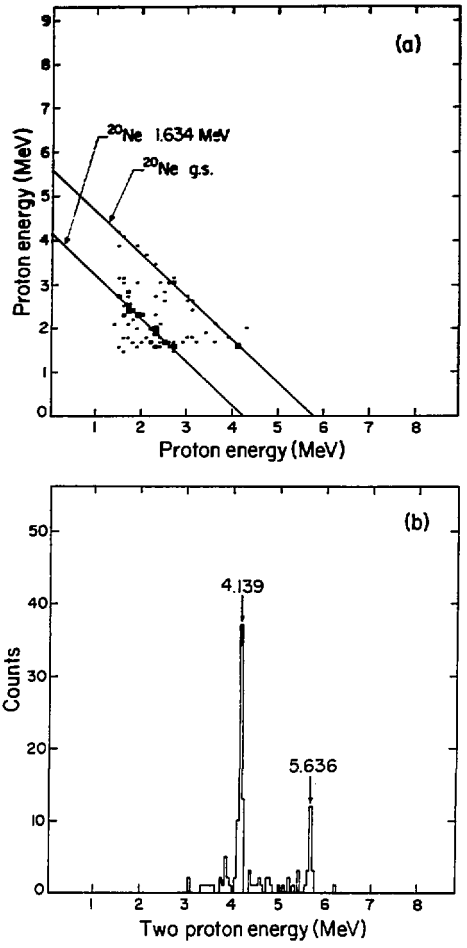

Fig. IV-3 (a) A proton-proton coincidence spectrum following the beta decay of ^{22}Al (E_p^L vs. E_p^R). Kinematic lines corresponding to decay to the ground state and to the first excited state of ^{20}Ne are shown.

(b) A summed energy spectrum for the two-proton coincidences in (a): $(E_p^L + E_p^R)$.

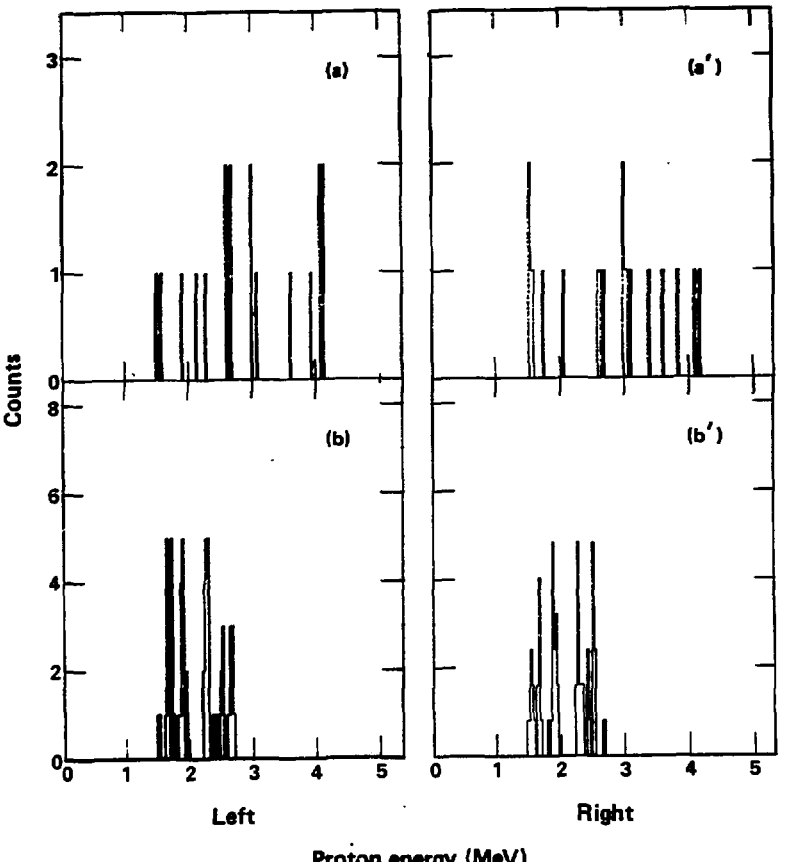

Fig. IV-4 Individual proton spectra obtained by gating on ^{22}Al two-proton summed energy groups. a, a' are gated on the 5.636 MeV group and are left and right telescope energies, respectively. b, b' are gated on the 4.139 MeV group.

Individual proton spectra corresponding to the 4.139 MeV and 5.636 MeV two-proton peaks are shown in Figure IV-4. These spectra are generated by placing a gate around the two-proton peak of interest and displaying the "left" and "right" telescopes. "Left" and "right" spectra for a given two-proton peak obtained in this manner are expected to be identical except for statistical variations and physical differences between the telescopes (such as different thresholds, etc.); these do appear to be identical within these limits.

Interpretation of the results, beyond the assignment of the groups observed, requires some consideration of the mechanism(s) for the emission of two protons from the intermediate T=2 state in ^{22}Mg. Two possibilities, as discussed in Section II-D, are A) single-step ^{2}He emission (two protons coupled to a $^{1}S_{0}$ configuration) or B) a sequential two-step process proceeding through an intermediate state (or states) in ^{21}Na.

Focusing on the stronger decay branch, ^{2}He emission to the first excited state of ^{20}Ne should occur predominantly within relative laboratory angles of ~40° (as evidenced, for example, by the distribution in ^{2}He break-up energies (ε) observed by Congedo et al. (Co80), which has the expected maximum at $\varepsilon \sim 0.5$ MeV, and by use of equation II-14). Sequential emission, in this case, is probably isotropic since it is likely that one of the protons comes from the 2s1d shell with ℓ=0. Since the telescope pair used in this experiment is capable of detecting protons at angles of 0-70°, it could observe proton coincidences originating from either mechanism. Individual proton energies arising from the former mechanism are expected to show

a distribution centered about $E_p^L = E_p^R$, with the observed shape of the distribution determined by the final state interaction and the detector configuration (see Appendix A for a discussion of detector efficiences as a function of η). Sequential emission, while still symmetric about $E_p^L = E_p^R$ (due to the detection method), would be expected to show distinct proton groups corresponding to transition energies through the intermediate state(s) in ^{21}Na.

Given only the proton-proton coincidence spectra shown, the mechanism for two-proton emission cannot be conclusively determined. The peak-like structure in the individual proton spectra for the first excited state transition seems to indicate at least a component of sequential emission and a complex decay scheme that could give rise to most of the major groups present in these spectra can indeed be constructed using some of the many known states in ^{21}Na. However, other data such as the two-proton to one-proton ratio discussed below and some notable differences between these spectra and those of a known sequential emission in ^{26}P decay (see Section IV-B) make it difficult to accept this decay as total sequential emission with any certainty. Observation of low statistics, continuous spectra (such as that expected from ^{2}He emission) has also, in the past, led to many heated discussions on the existence (or non-existence) of peaks. Finite detector resolution and uncertainties in detector efficiency variance with η will affect spectrum appearance for either mechanism. While it seems likely that at least some of this decay proceeds by sequential emission, the possibility of a component of ^{2}He emission (or some other mechanism not yet considered) cannot be excluded. The

above discussion also applies to the spectra obtained from the ground state transition with the further observation that this case is even less determinable.

The calculation of the relative intensity of two-proton to one-proton emission (2p/1p) from $^{22}Mg^*$ (using only the 4.139 MeV two-proton group and the 7.839 MeV single-proton group observed in the $\Delta E1+\Delta E2+E$ spectrum) is dependent on the assumed mechanism since the detector arrangement has an efficiency dependent on the angular correlation of the protons (see Appendix A). If an isotropic sequential distribution is assumed, 2p/1p = 1.5 whereas if all events are assumed to be emitted at a laboratory angle of 40° (^2He), 2p/1p = 0.3. (These values are also dependent on the observable individual proton energy range detectable by the telescopes). Since for sequential emission, this 2p/1p ratio is affected by the relative penetrabilities of the 7.839 MeV single-proton and the first sequential proton (energy < 4.139 MeV) 2p/1p = 1.5 seems high, whereas 2p/1p = 0.3 may be a reasonable value for ^2He emission. This result would tend to indicate at least a substantial component of ^2He emission; however, it must be realized that if sequential emission proceeds through several intermediate states the two-proton branch will be the sum of the individual branches to all these states. If sufficient states are involved (and the individual proton spectra seem to indicate several states if it is sequential) this ratio might also be reasonable for sequential emission.

B. ^{26}P decay

^{26}P was produced via the $^{28}Si(^{3}He,p4n)^{26}P$ reaction with 110-130 MeV $^{3}He^{+2}$ beams of 3-7 μA intensities. All ^{26}P work was done with the single target, single capillary system described in Section III-A, using a rotating wheel as a catcher.

1) Single-proton data

Proton spectra obtained with a three-element telescope as described in Section III-B (110 μm ΔE1, 60 μm ΔE2, 500 μm E, 2.3% of 4π sr) are shown in Figure IV-5. The dominant features of each spectrum are due to beta-delayed protons from the decays of ^{21}Mg, ^{25}Si and ^{29}S produced via high yield ($^{3}He,x\alpha 2n$) reactions. At 60 MeV, which is below the threshold of 63.5 MeV for ^{26}P production, two previously unknown proton groups, probably from ^{29}S decay (assigned by additional low energy bombardments on several targets), are observed at laboratory energies of 7.114±0.015 MeV and 7.581±0.015 MeV. At 110 MeV, a new group is observed at a laboratory energy of 7.269±0.015 MeV in addition to the ^{29}S groups. In order to reduce the amount of ^{29}S ($t_{1/2}$=187 ms) in the spectrum, another measurement was made A) at 130 MeV and B) with the wheel speed increased to ~2 cm/s to discriminate against longer-lived activities. The resulting spectrum (Figure IV-5(a)) shows that the ^{29}S contribution is reduced and the new group at 7.269 MeV is more pronounced. Also present is a group at 6.827±0.050 MeV which will be discussed further below.

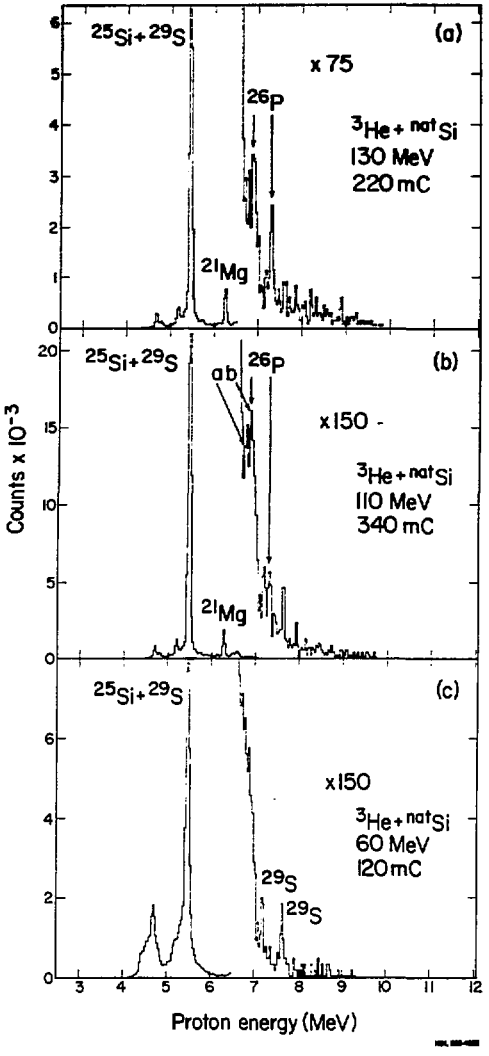

Fig. IV-5 Beta-delayed single-proton spectra. The spacing between the arrows labeled ^{26}P is calculated from the known energy difference between the ground state and first excited state of ^{25}Al (see text).

As shown in Figure IV-6, the 7.269±0.015 MeV group can be attributed to the isospin forbidden decay of the lowest T=2 state in ^{26}Si (fed by the superallowed beta-decay of the T=2 ground state of ^{26}P) to the ground state of ^{25}Al. (As noted below, this assignment is consistent with Coulomb displacement energy considerations). The J^{π} assignment of 3^{+} to the levels in this isospin multiplet is based on the measurement of the hyperfine splitting of the T_z=+2 member, ^{26}Na, by Huber et al. (Hu78).

The known energy difference between the ^{25}Al ground state and its first excited state (En78) permits the calculation of the proton energy to be expected if decay to the first excited state also occurs. This energy is 6.835±0.015 MeV and is indicated in Figure IV-5(a) and IV-5(b) with the arrow at the lower proton energy. Accurate measurements in this region of the spectrum are made extremely difficult by the high "background" caused by the following effects: A) a distortion to higher energies of the very intense lower energy proton groups caused by simultaneous detection of the proton and the preceding positron (see Section III-B) and B) the actual presence of some weak groups from T_z=-3/2 beta-delayed proton emitters. The latter accounts for the two groups labeled a and b in Figure IV-5(b), which are also observed in low energy bombardments of Mg targets and can be tentatively assigned to the decay of ^{25}Si. In Figure IV-5(a), however, the ^{25}Si ($t_{1/2}$=218 ms) contribution is substantially reduced and the relative intensity of the peak observed at 6.827±0.050 MeV is consistent with a major component of that peak arising from decay of the ^{26}Si, T=2 state to the first excited state

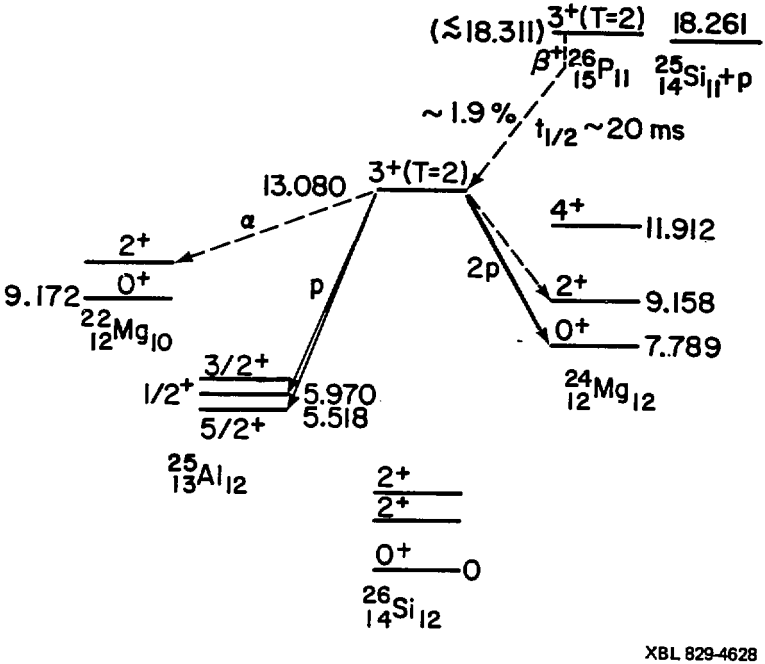

Fig. IV-6 Proposed partial decay scheme for ^{26}P.

of ^{25}Al.

In order to confirm the assignment of these proton groups to the decay of ^{26}P, the cross-bombardment $^{27}Al(^{3}He,4n)^{26}P$ was also investigated. Despite the poor spectrum quality caused by the expected decreased yield of ^{26}P, it appears that both the 7.269 MeV and 6.827 MeV proton groups are again present with yield reduced by a factor of five (see Figure IV-7). The possible reappearance of the 7.114 MeV group that was tentatively assigned to ^{29}S decay clouds this assignment; however, all data except this spectrum are consistent with the assignment. In any event, assignment of this group does not affect interpretation of the ^{26}P decay since it definitely does not arise from decay of this isotope (compare Figures IV-5(a) and IV-5(b)). Appearance of the 7.269 and 6.827 MeV groups, despite low spectrum quality, is supporting evidence for the elimination of sulfur isotopes (in particular the unknown isotope, ^{27}S) as a source of this activity. Arguments similar to those in the ^{22}Al discussion for the elimination of ^{23}Si are also applicable in this case. Coupled with the previous work described in Section IV-A, this shows that only ^{26}P can be a source of these proton groups.

A rough half-life of 20^{+35}_{-15} ms was determined for the 7.269 MeV proton group by varying the wheel rotational speed and observing the relative yields of the various activities present (see Appendix B). This method could, in principle, yield a precise half-life measurement but does not do so here due to the low yield of ^{26}P. A shell model calculation by Wildenthal (Wi82) for the beta decay of ^{26}P using allowed branches to states up to 9 MeV in excitation in ^{26}Si and the

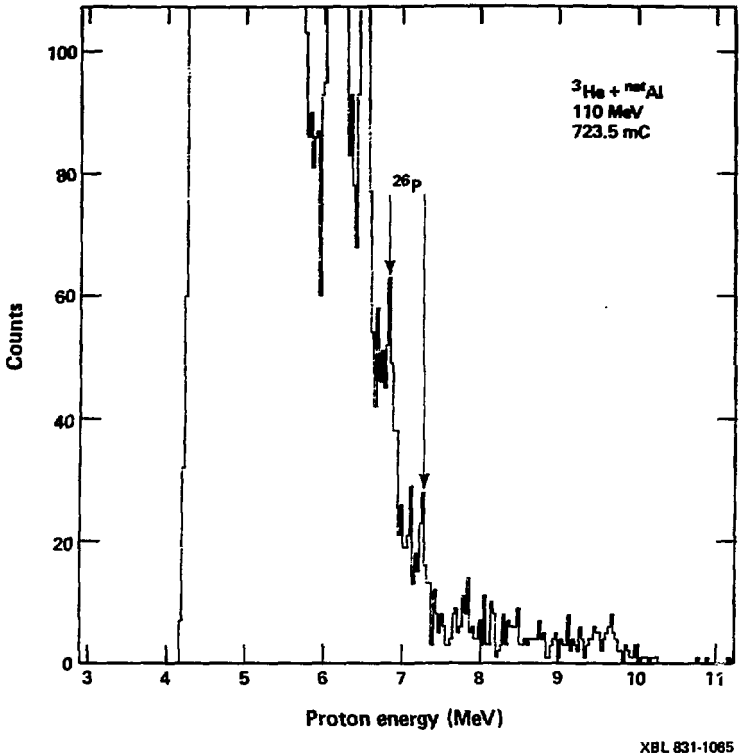

Fig. IV-7 Cross-bombardment spectrum for ^{26}P. Location of arrows is that of ^{26}P peaks observed in a ^{28}Si bombardment.

superallowed branch yields a predicted half-life of 22 ms. (This should be considered an upper limit on the expected half-life since there will be some contributions from decays to levels above 9 MeV).

Assuming a pure Fermi log ft of 3.19 (the Gamow-Teller contribution should be negligible, see Section II-B) and using the observed half-life of 20 ms gives a super-allowed branch of $1.9^{+3.5}_{-1.4}$%. Comparison of the ^{26}P yield to the other activities present in the ^{3}He bombardments indicates an effective cross section for the 7.269 MeV proton group of 1.8 nb (within a factor of three) which corresponds to a lower limit of the total production cross-section of 100nb. This is a lower limit since not all of the decay proceeds by single-proton emission (see Section IV-B(2)).

The center of mass proton energy of the group decaying to the ground state of ^{25}Al, taken together with the ^{25}Al mass (Wa82), gives a mass excess of 5.936±0.015 MeV for the lowest T=2 state in ^{26}Si (an excitation energy of 13.080±0.015 MeV). As discussed in Section II-A, the ^{26}P ground state mass is of interest since this nuclide is thought to be at or beyond the limit of particle stability. An estimate of the Coulomb displacement between this analog state and the ^{26}P ground state can give an estimate for the latter's mass. A simple size correction (assuming an $A^{1/3}$ dependence) to the known T=3/2, ^{27}Si* - ^{27}P Coulomb difference (Be77) gives a value of 11.013±0.038 MeV (the indicated error is only from known errors of the masses involved) for the ^{26}P ground state mass excess. This value indicates ^{26}P would be bound to direct proton emission by 104 keV. However, if one predicts the ^{26}P mass

from a Kelson-Garvey type calculation (all masses from (Wa82)), this indicates ^{26}P would be unbound by 73 keV. A significant Thomas-Ehrman shift is to be expected in ^{26}P and such a shift should cause the ^{26}P mass to be lower than that indicated by a Kelson-Garvey calculation (and would also affect the CDE estimate above).

In order to provide a limit for the ^{26}P mass, the barrier penetration code, COCAG (Se73), was used to estimate the maximum energy available for ℓ=0 proton emission which still permits beta decay to dominate (see Section II-C). The conclusion from this is indicated in Figure IV-6; ^{26}P can at least be up to 50 keV unbound and it would not significantly affect any of our observations.

2) Two-proton data

Single-proton data discussed in the previous section gave a mass excess for the lowest T=2 state in ^{26}Si of 5.936±0.015 MeV. Figure IV-6 shows that this value indicates this T=2 level is unbound to two-proton emission by 5.291 MeV.

Two-proton spectra obtained following a 600 mC bombardment by methods discussed in Section III are shown in Figure IV-8 and IV-9. As discussed for the ^{22}Al work, all events in these spectra are fast (20 ns) proton-proton coincidences and only about one random event is expected to be present. Since ^{26}P is produced with 110 MeV ^{3}He bombardment of silicon targets, it is possible to produce ^{22}Al and ^{26}P simultaneously. The two-proton summed energy spectrum shown in Figure IV-8(b) does contain groups from the decay of both isotopes (compare to Figure IV-3(b)). The two-proton group at 4.927±0.020 MeV

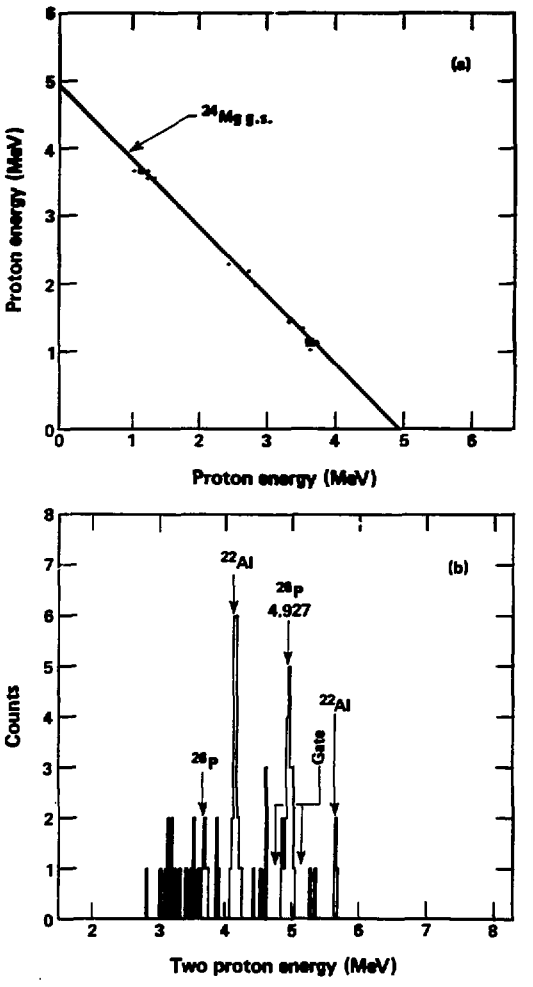

Fig. IV-8 (a) A proton-proton coincidence spectrum following the beta decay of ^{26}P (E_p^L VS. E_p^R). Spectrum is gated as shown in part (b).

(b) A summed energy spectrum for two-proton coincidences obtained following the beta decays of ^{26}P and ^{22}Al (see text).

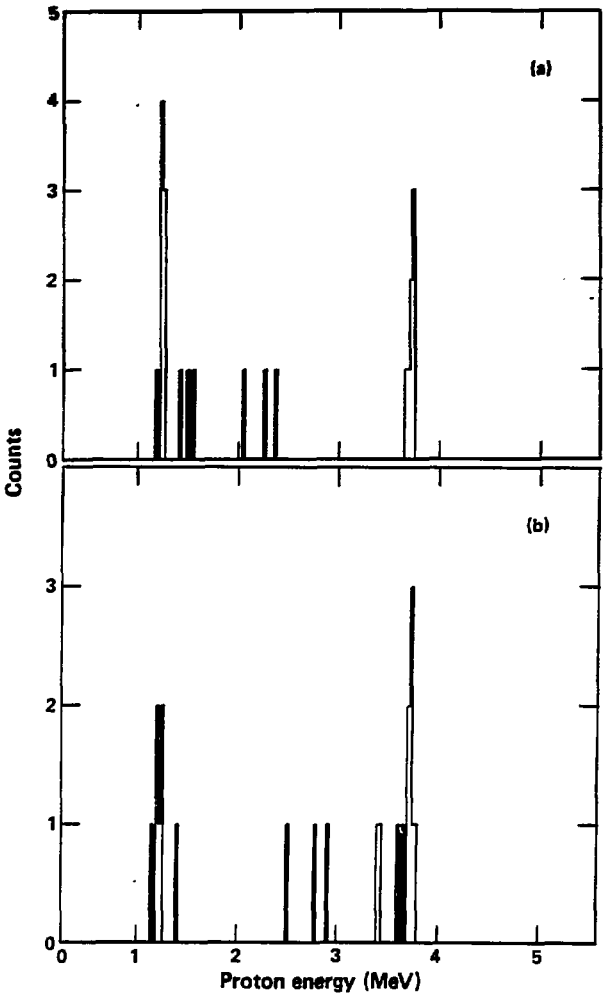

Fig. IV-9 Individual proton spectra from left and right telescopes corresponding to two-proton emission to the ground state of ^{24}Mg (see gate in Fig. IV-8(b)).

shown in Figure IV-8(b) corresponds to the decay of the T=2 analog state of ^{26}Si (fed by the superallowed beta decay of ^{26}P) to the ground state of ^{24}Mg (see Figure IV-6). The lower energy arrow labeled ^{26}P in this spectrum is located at the approximate expected energy for the two-proton group corresponding to the decay to the ^{24}Mg first excited state.

As evidenced by Figures IV-2 and IV-6, the ^{22}Al and ^{26}P decays are very similar, however, there is one notable difference. Since the T=2 analog state in ^{26}Si is expected to be 3^+, decay by ^{2}He emission ($J^\pi=0^+$ particle) is spin-parity forbidden to the ground state of ^{24}Mg. Therefore, the observed decay to this state is expected to be sequential. A gate set on this group (as shown in Figure IV-8(b)) produced the individual proton energy spectra shown in Figures IV-8(a) and IV-9. These spectra do have the expected appearance of a sequential emission through one state in ^{25}Al; however, it is not known which proton group of the two observed (laboratory energies 1.210±0.015, 3.699±0.015 MeV) corresponds to the first proton emitted. It is likely that the higher energy group at 3.699 MeV is emitted first (from penetrability arguments) and if this is the case a possible intermediate state in ^{25}Al is a known $7/2^-$ state at 3.696 MeV excitation (En78).

The relative intensity of the 4.927 MeV two-proton group to that of the 7.269 MeV ^{26}P single-proton group can be calculated. Assuming, for simplicity, isotropic sequential emission and using detector efficiencies calculated as described in Appendix A, a value of 2p/1p=0.7 is obtained. For comparison of this value with that of

^{22}Al it should be noted that the ground state single-proton group used here is not necessarily the most intense group (the ground state group in ^{22}Al is considerably less intense than the first excited state group); however, since it is the *only* clearly observable ^{26}p group, it is used to obtain this value.

V. Summary and Conclusions

Decays of the odd-odd, $T_z = -2$ nuclei ^{22}Al and ^{26}P have been observed, establishing the existence of these previously unknown isotopes. The measured half-lives indicate both nuclides decay predominantly by beta decay.

Both beta-delayed single-proton and beta-delayed two-proton emission were observed for each isotope with the latter decay mode being a previously unobserved form of radioactivity. Single-proton studies permitted measurement of the masses of the lowest $T = 2$ analog state in the beta decay daughters, ^{22}Mg and ^{26}Si, and a rough determination of the beta decay half-lives. The masses of these levels not only provide additional information for studies of charge dependent effects in nuclei but also confirmed the prediction that these states were unbound to two-proton emission by 5-6 MeV. Subsequent proton-proton coincidence experiments provided measurements of the beta-delayed two-proton spectra of both ^{22}Al and ^{26}P.

With the observation of beta-delayed two-proton emission came the possibility of detailed studies on the mechanism of two-nucleon emission. Beta-delayed two-neutron decay, the analogous process for neutron rich nuclei, has been known for several years (Az79); however, difficulties associated with detection of uncharged decay products have hindered studies of its mechanism. Individual proton spectra have shown that the ^{26}P beta-delayed two-proton emission to the ^{24}Mg ground state very likely proceeds by the expected sequential process with only the order of the sequence being uncertain. The situation for ^{22}Al decay is less clear: it is probable that at least

some sequential emission occurs but this decay can not be conclusively characterized from the data presented.

Further experiments of interest would be acquisition of spectra with higher statistics for both isotopes (with particular interest in observation of the ^{26}P beta-delayed two-proton emission to the ^{24}Mg first excited state for a comparison to the ground state branch) and also the measurement of the two-proton decay of both nuclei at a large relative proton angle, θ_{rel}. The latter experiment has the possibility of excluding most ^{2}He events, thereby clarifying the decay mechanism. Additionally, as shown in equation II-15, the second proton in a sequential decay should show a measurable difference in its laboratory energy, permitting determination of the order of emission of the protons in the resulting sequential spectrum.

If ^{2}He emission can be identified in these decays, it could provide a new method for studies of the nuclear force since such data would provide the initial case(s) of two strongly interacting particles being simultaneously emitted in a nuclear decay. Beta-delayed two-proton emission by any mechanism may also eventually serve as a useful spectroscopic tool in cases where beta-delayed single-protons of interest are obscured by competing activities. Further studies of ^{22}Al and ^{26}P, and additionally, other expected beta-delayed two-proton emitters, would seem to be a potentially exciting, new line of research.

Appendix A: Detector efficiencies

It is frequently necessary to have a value for the fraction of the events (for both single-proton and two-proton work) that are detected out of the total number occurring. For the single-proton work, if a centered point source is assumed, this is a simple calculation and yields the expression

$$F = \frac{1-\cos\theta}{2} \qquad (A-1)$$

where θ is the half angle of the right circular cone defined by the edge of a circular detector and the point source (located on the centerline of the telescope). As more complex detector arrangements are used and as possible proton-proton angular correlations are considered for the two-proton work, these calculations become considerably more complex. For these complex configurations, even if it is possible to derive an analytical expression (and sometimes it's difficult to say whether a solution is even possible!), it is frequently simpler to use computer techniques to calculate detector efficiencies.

Two standard techniques that are used are Monte Carlo and mapping techniques. For all the calculations described below, mapping techniques were used since the solution can be made arbitrarily accurate and there is no question of statistical uncertainty. The problems encountered could also have been readily solved by Monte Carlo methods.

The first case that will be discussed is that of the

single-proton telescope for a point source that is not on the telescope axis. This problem's solution is desirable since the rotating catcher wheel constantly carried activity away from this axis. For half-life measurements, described in Appendix B, an expression E(x) for detector efficiency as a function of the distance from the axis, x, is needed. An analytic expression is probably possible for this case, but it was simpler to use the program, WHELIF (Ca82), which calculates E for given values of x by a mapping technique. It can then be seen that E(x) is approximately linear over the region of interest for the single-proton telescope used in this work (see Figure A-1). This information was all that was required for the half-life measurements; however, E(x) could also be used to make non-point source corrections if desired. For this work, detector efficiencies of that accuracy were never necessary.

More difficult problems are encountered when two-proton detection efficiencies are considered. Sequential emission is still quite simple but ^{2}He emission is more complex. Considering sequential first, and making the assumption that the two protons are both emitted isotropically, it is easy to show that

$$F_{seq} = 2 \cdot \left(\frac{F}{2}\right)^2 \qquad (A-2)$$

where F is defined in equation A-1. This expression arises since each side of the two-proton telescope has a detection efficiency of F/2 and there are two possible ways for the protons to be detected.

For ^{2}He detection efficiency, a program called GEOM2P (Ca82) was written. This program works on a mapping technique and produces a

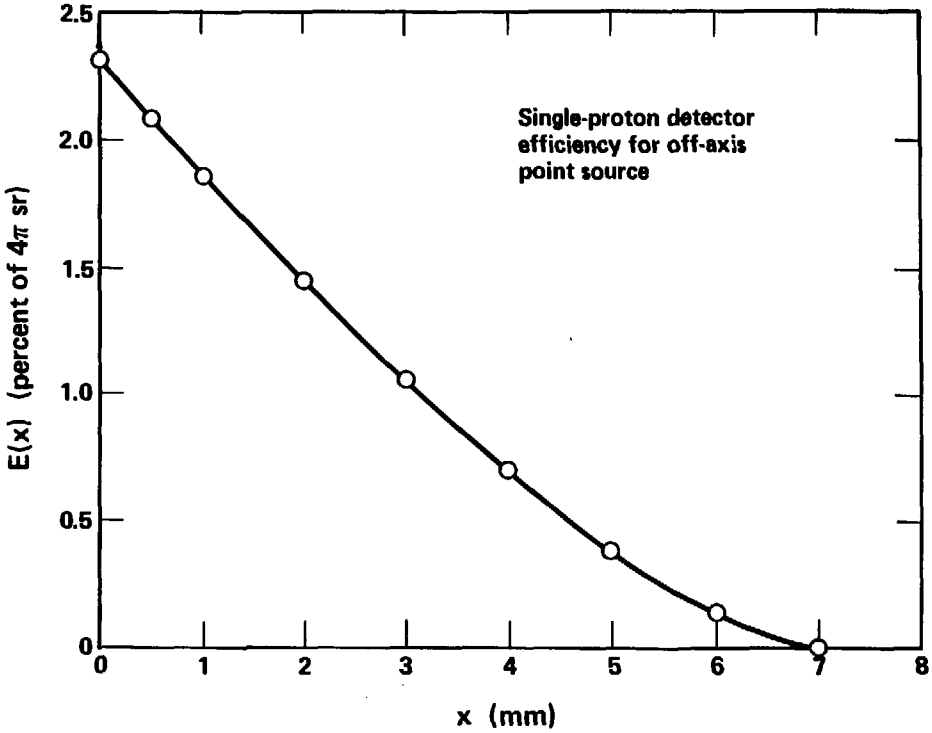

XBL 831-1072

Fig. A-1 Single-proton telescope detection efficiency calculated as a function of source distance from telescope axis (see text).

value G_{2p} that is the probability of detection of the "second" proton given detection of one of the protons in the "reference" side. G_{2p} is calculated only as a function of η so any information on the distribution of η must be added externally. If all ^{2}He are assumed to break up at a fixed angle η (and this is probably a reasonable approximation if η is fixed at its most probable value, η_{max}; see Section II-D) detector efficiency is given by

$$F_{2_{He}} = 2 \cdot \frac{F}{2} \cdot G_{2p} \qquad (A-3)$$

Figure A-2 shows this quantity plotted for ^{22}Al as a function of F/2 (percent of 4π sr/side) for a variety of ε values assuming for each ε that η is fixed at the most probable (maximum) value. The curves plotted are for the beta-delayed two-proton decay of ^{22}Al to the first excited state of ^{20}Ne. Reaction work (for example, (Co80)) has shown that $\varepsilon \sim 500$ keV is the most probable value, producing a value of $\eta \sim 40^\circ$. These assumptions were used for calculation of the 2p/1p ratio in Section IV.

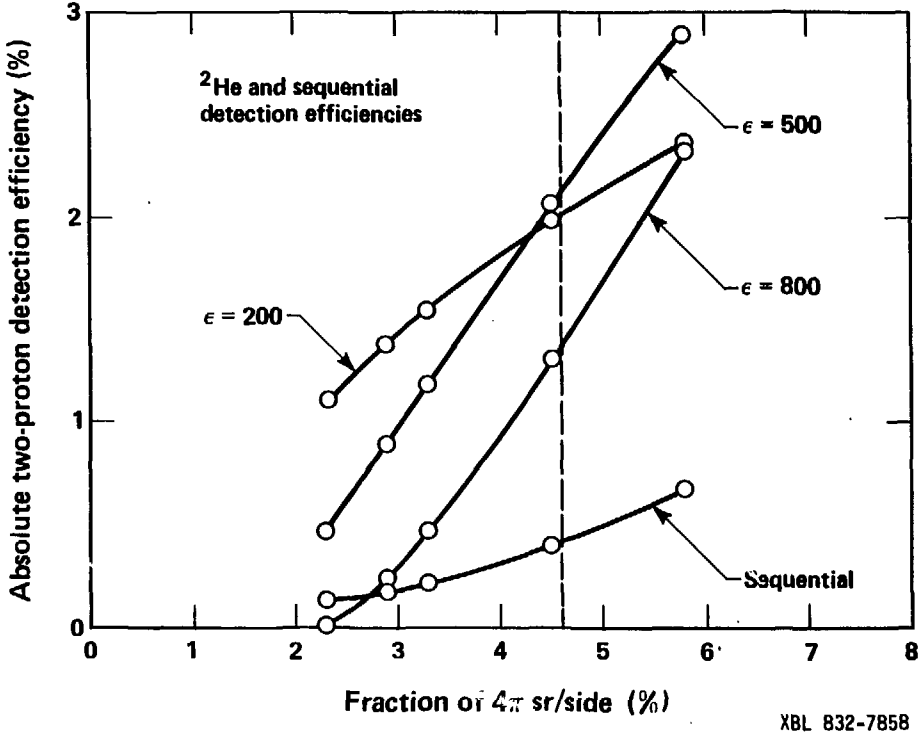

XBL 832-7858

Fig. A-2 Two-proton detector efficiencies calculated as functions of solid angle of individual telescopes. Dashed line is the value for the two-proton telescope used in this work. η is assumed fixed at η_{max} for the value of ϵ (in kev) indicated.

Appendix B: Half-life measurment techniques

Most systems for beta-decay half-life measurements involve some sort of production and counting cycle; those used with helium jets usually rely on a mechanical motion of the counting source or some type of shutter. In addition to the difficulties involved with construction of mechanical devices that move rapidly enough to be of use for short half-life measurements, these types of systems have large "dead times" associated with them due to lack of continuous counting of the source. Since for the work described a half-life measurement was of secondary importance, two techniques described below were used that did not lower the absolute yield of activity greatly, while still giving at least some half-life information.

If a stationary catcher is used, the only "half-life losses" of activity occur in transit by the helium jet. If this transit time, τ, is varied and the change in half-life losses is observed it is possible to measure a half-life. In practice, two reference half-lives are used as a "clock" to monitor the changes in τ. The ratio of the amount of each activity, λ_1 and λ_2, that is detected is denoted $R(\tau)$. If the transit time τ is changed by an amount $\Delta\tau$, the following expression arises:

$$\frac{R(\tau)}{R(\tau+\Delta\tau)} = e^{(\lambda_1-\lambda_2)(\Delta\tau)} \qquad \text{(B-1)}$$

Since, in general, τ is not known, equation B-1 can be used to obtain $\Delta\tau$ if R is measured with a system operating with transit time τ and again measured at $\tau+\Delta\tau$. τ is most easily varied physically by

changing the operating conditions of the helium jet, i.e., pressure, capillary diameter, etc.

A third, unknown activity, λ_3, can now be measured using the known $\Delta\tau$ and equation B-1 with the activity, λ_3, referenced against either λ_1 or λ_2. The major problem with this technique is the assumption of discrete transit time, τ. Helium jet transit times are not, in general, well understood and while a discrete τ is probably a good approximation, it is known that this is not exact. There are fast and slow components in helium jet transit time and a better treatment would be to use a distribution, $P(\tau)$, if more were known about it. Uncertainties in this distribution contribute to the large errors associated with the ^{42}Al half-life, discussed in Section IV, for which this technique was used.

A better technique is to collect the activity on a rotating catcher wheel and vary the wheel speed. Again, if two reference activities are measured, a third half-life can be determined. For this case, the activities are counted for some time τ before being rotated "out of sight" of the detector. If a bombardment is done with a fast and a slow wheel speed, the reference activities can be used to determine the times, τ_f and τ_s, using

$$\frac{N_s^i}{N_f^i} = K\left(\frac{1-e^{-\lambda_i \tau_s}}{1-e^{-\lambda_i \tau_f}}\right)\frac{P(\tau_s)}{P(\tau_f)} \qquad (B\text{-}2)$$

$$P(\tau) = \frac{\int_o^\tau e^{-\lambda t} E(t)dt}{\int_o^\tau e^{-\lambda t} dt}$$

where: N_s^i, N_f^i = number of decays observed in slow, fast bombardments

K = normalization for differing bombardment lengths

Two activities, λ_1 and λ_2, provide two equations that can be solved (numerically) for τ_s, τ_f. $P(\tau)$ is a correction tnat is made if counter efficiency, E, is not constant with time between 0 and τ, where τ is now defined as the point at which E goes to zero (i.e., "out of sight" of detector). For the single- proton telescope used in tnis work, E(t) is not constant since the activity is being moved away from the detector axis and, as discussed in Appendix A, this reduces the detection efficiency. Appendix A shows tnat E(t) can be treated as an approximately linearly decreasing function from 0 to τ (see Figure A-1). If wheel speed is known, and also full information on detector solid angles, etc., is available, τ_s and τ_f can be calculated; however, uncertainties in this information make it better to use the reference activities to determine τ_s and τ_f. If the linear E(t) approximation is used, equation B-2 becomes:

$$\frac{N_s^i}{N_f^i} = K \frac{{}_f(e^{-\lambda_i \tau_s} + \lambda_i \tau_s - 1)}{{}_s(e^{-\lambda_i \tau_f} + \lambda_i \tau_f - 1)} \qquad \text{(B-3)}$$

Numerical solution of tne above equation for the reference activities provides τ_s and τ_f; subsequent solution for

the third activity, λ_3, provides the unknown half-life. This technique was used for the ^{26}P half-life measurement discussed in Section IV. The error on this measurement is at least as large as that on ^{22}Al, but in this case the error is attributable to the relatively small amounts of ^{26}P and large amounts of background activities.

Appendix C: Two-proton detector calibration; addition of detectors

For the two-proton sum spectra shown in this work, it is desirable to have a calibration producing two-proton energy as a function of channel number. Since there are no reference two-proton peaks, a calibration can not be directly obtained in the usual way in which reference peaks and their corresponding channel numbers are merely fitted to a line. However, each individual telescope can be well calibrated using single-proton groups and this is all that is actually necessary.

If two detectors (or detector telescopes), 1 and 2 are calibrated such that

$$E_1 = a_1c_1+b_1 \qquad (C\text{-}1)$$

$$E_2 = a_2c_2+b_2$$

where

E_i = energy

c_i = channel number

a_i = gain

b_i = offset

and a sum spectrum is created such that

$$c = N\,\frac{c_1}{k} + c_2 \qquad (C\text{-}2)$$

where $k = a_2/a_1$

N = normalization (arbitrary)

then the calibration of this new sum spectrum will be

$$E = ac+b \qquad \text{(C-3)}$$

where

$$a = a_2/N$$

$$b = b_1 + b_2$$

For the two-proton telescope described in Section III, the values described by equation C-1 were obtained from known groups of $T_z=-3/2$ isotopes. The spectrum described in equation C-2 is easily created in the program,
CHAOS, and its calibration is obtained using equation C-3.

Detector addition also occurs in the original creation of the telescope total energy spectra ($\Delta E1 + \Delta E2$) and this addition is also described by the above equations. In this case, however, it is really only necessary to determine k to ensure a linear calibration since the single-proton total energy spectrum is directly calibrated. A value for k was usually determined using alpha sources and/or precision pulsers.

Acknowledgments

I would like to express my thanks to:

My research director, Professor Joseph Cerny, for his support and endless enthusiasm for all the projects on which I have worked over the years;

Past and present members of the Cerny research group, in particular: Dr. Juha Aysto and Dr. Peter Haustein, for their help and instruction in my early years as a grad student; grad students (and former grad students) Dr. Alden Bice, Dr. Dennis Moltz, near-Dr. Roger Parry and Dr. Jan Wouters for general help; visiting scientists Dr. Jorma Honkanen, Zong Yuan Zhou and Dr. Shu Hua Zhou for help in planning and carrying out the work described in this thesis; and Claude Ellsworth for experimental set-up, target making and general handling of loose ends;

Professor B. H. Wildenthal for useful discussions and theoretical calculations;

Dr. B. Jonson for a particularly helpful phone call last year;

Jack Walton and the rest of the silicon lab for quality, custom-made detectors;

Dr. Creve Maples and his staff, Bill Ratnbun, Dan Weaver, and Elinor Potter for providing and frequently assisting with my use of a fine on-line data collection and analysis system that was critically needed for this work;

The cyclotron crew and staff of "the 88" for providing excellent beams;

The cyclotron accelerator technicians for quality construction of the many strange devices I've needed (often on very short notice);

Roy Burton for frequently inspired mechanical design, and teaching me the fundamentals;

Carol Adams and Wanda Smith for general help and typing (in particular, for typing this thesis);

And finally, most of all, my wife, Dana, who with a full-time job, night classes, taking care of me, and generally putting up with life as it is married to a grad student, had a much more challenging task than mine. Thank you, for your love, patience and support through the years.

REFERENCES

(Ay 81) J. Aysto, M. D. Cable, R. F. Parry, J. M. Wouters, D. M. Moltz, and J. Cerny, Phys. Rev. C23 (1981) 879.

(Az 79) R. E. Azuma, L. C. Carraz, P. G. Hansen, B. Jonson, K.-L. Kratz, S. Mattsson, G. Nyman, H. Ohm, H. L. Ravn, A. Schroder, and W. Ziegert, Phys. Rev. Lett. 43 (1979) 1652.

(Be 77) W. Benenson, D. Mueller, E. Kashy, H. Nann, and L. W. Robinson, Phys. Rev. C15 (1977) 1187.

(Bl 76) M. Blann, ERDA Rep. No. COO-3494-29 (1976).

(Ca 82) Program written by M. D. Cable.

(Co 80) T. V. Congedo, I. S. Lee-Fan, and B. L. Cohen, Phys. Rev. C22 (1980) 985.

(Da 74) C. N. Davids, D. R. Goosman, D. E. Alburger, A. Gallmann, G. Guillaume, D. H. Wilkinson, and W. A. Lanford, Phys. Rev. C9 (1974) 216.

(En 78) P. M. Endt and C. van der Leun, Nucl. Phys. A310 (1978) 1.

(Go 64) F. S. Goulding, D. A. Landis, J. Cerny, and R. H. Pehl, Nucl. Instr. and Meth. 31 (1964) 1.

(Go 66) V. I. Gol'danskii, Usp. Fiz. Nauk. 87 (1965) 255; Sov. Phys. Uspekhi 8 (1966) 770.

(Go 80) V. I. Gol'danskii, Pisma Zh. Eksp. Teor. Fiz 32 (1980) 572; JETP Lett. 32 (1980) 554.

(Ha 69) J. C. Hardy, H. Brunnader, J. Cerny and J. Janecke, Phys. Rev. 183 (1969) 854.

(Hu 78) G. Huber, F. Touchard, S. Buttgenbach, C. Thibault, R. Klapisch, H. T. Duong, S. Liberman, J. Pinard, J. L. Vialle, P. Juncar, and P. Jacquinot, Phys. Rev. C18 (1978) 2342.

(Ja 70) W. Jaus and G. Rasche, Nucl. Phys. A143 (1970) 202.

(Ja 72) W. Jaus, Phys. Lett. 40 (1972) 616.

(Ke 66) I. Kelson and G. T. Garvey, Phys. Lett. 23 (1966) 689.

(La 58) A. M. Lane and R. G. Thomas, Rev. of Mod. Phys. 30 (1958) 257.

(Ma 68) J. B. Marion and F. C. Young, Nuclear Reaction Analysis-Graphs and Tables (North-Holland, Amsterdam, 1968) p. 327.

(Ma 79) C. Maples and J. Sivak, IEEE Trans. Nucl. Sci. NS-26 (1979) 4409.

(Mc 82) Program written by R. J. McDonald.

(Mo 80) D. M. Moltz, J. M. Wouters, J. Aysto, M. D. Cable, R. F. Parry, R. D. von Dincklage and J. Cerny, Nucl. Instr. and Meth. 172 (1980) 519.

(Mo 81) D. M. Moltz, J. Aysto, M. D. Cable, R. F. Parry, P. E. Haustein, J. M. Wouters, and J. Cerny, Nucl. Instr. and Meth. 186 (1981) 141.

(On 65) G. G. Ohlsen, Nucl. Instr. and Meth. 37 (1965) 240.

(Ra 78) S. Raman, T. A. Walkiewicz, and H. Behrens, At. Data and Nucl. Data Tables 16 (1975) 451.

(Se 73) R. G. Sextro, Ph.D. thesis, Lawrence Berkeley Laboratory Rept. No. LBL-2360 (1973).

(St 69) R. H. Stokes and P. G. Young, Phys. Rev. 178 (1969) 1789.

(St 79) D. P. Stahel, Ph. D. Thesis, Lawrence Berkeley Laboratory Rept. No. LBL-9706 (1979).

(Sy 71) K. R. Symon, Mechanics, (Addison-Wesley, Reading, MA, 1971) p. 175-182.

(To 77) I. S. Towner, J. C. Hardy, and M. Harvey, Nucl. Phys. A284 (1977) 269.

(Wa 77) A. H. Wapstra and K. Bos, At. Data and Nucl. Data Tables 19 (1977) 175.

(Wa 82) A. H. Wapstra, G. Audi and K. Bos, January 1982 Atomic Mass Tables for Nuclides.

(Wi 57) E. P. Wigner, in Proceedings of the Robert A. Welch Foundation Conference on Chemical Research, Houston, 1957, edited by W. O. Milligan, p. 67 (unpublished).

(Wi 70) D. H. Wilkinson and B. E. F. Macefield, Nucl. Phys. A158 (1970) 110.

(Wi 74) D. H. Wilkinson and B. E. F. Macefield, Nucl. Phys. A232 (1974) 58.

(Wi 82) B. H. Wildenthal, private communication.

(Wo 82) Program written by J. M. Wouters.